

Nucleon Resonances with Hidden Charm in γp reactions

Jia-Jun Wu,¹ T.-S. H. Lee,² and Bing-Song Zou³

¹*School of Physical Sciences, University of Chinese Academy of Sciences(UCAS), Beijing 100049, China*

²*Physics Division, Argonne National Laboratory, Argonne, Illinois 60439, USA*

³*CAS Key Laboratory of Theoretical Physics, Institute of Theoretical Physics, Chinese Academy of Sciences, Beijing 100190, China*

Abstract

The excitations of nucleon resonances with hidden charm, $N_{c\bar{c}}^*$, in the γp reactions are investigated by using the predictions from the available meson-baryons (MB) coupled-channel models of $N_{c\bar{c}}^*$ with $MB = \rho N, \omega N, J/\psi N, \bar{D}\Lambda_c, \bar{D}^*\Lambda_c, \bar{D}\Sigma_c, \bar{D}^*\Sigma_c, \bar{D}\Sigma_c^*$. For the $\gamma p \rightarrow J/\psi p$ process, we first apply the Model of Donnachie and Landshoff to calculate the Pomeron-exchange amplitudes with the parameters determined from fitting the available total cross section data up to invariant mass $W = 300$ GeV. We then add the resonant $\gamma p \rightarrow N_{c\bar{c}}^* \rightarrow J/\psi p$ amplitudes to examine the effects of $N_{c\bar{c}}^*$ excitations on the cross sections of $\gamma p \rightarrow J/\psi p$ in the near threshold energy region covered by the recent experiments at Jefferson Laboratory. The $N_{c\bar{c}}^* \rightarrow MB$ transition matrix elements are determined from the partial decay widths predicted by the considered meson-baryons coupled-channel models of $N_{c\bar{c}}^*$. The $\gamma p \rightarrow N_{c\bar{c}}^*$ transition amplitudes are calculated from the Vector Meson Dominance (VMD) model as $\gamma p \rightarrow Vp \rightarrow N_{c\bar{c}}^*$ with $V = \rho, \omega, J/\psi$. The total $\gamma p \rightarrow J/\psi p$ amplitudes then depend on an off-shell form factor, parameterized as $F_V(q^2) = \Lambda^4/(\Lambda^4 + (q^2 - m_V^2)^2)$, which is needed to account for the q^2 -dependence of the photon-vector meson coupling constant $\frac{em_V^2}{f_V}$ of the VMD model. It has been found that with $\Lambda = 0.55$ GeV, the predicted total cross sections are within the range of the data in the energy region near the J/ψ production threshold. We then demonstrate that the $N_{c\bar{c}}^*$ can be most easily identified in the differential cross sections at large angles where the contribution from Pomeron-exchange becomes negligible. With the same VMD model and the same coupled-channel models of $N_{c\bar{c}}^*$, we also calculate the resonant amplitudes for the $\gamma p \rightarrow Vp \rightarrow N_{c\bar{c}}^* \rightarrow \bar{D}^0\Lambda_c^+(\bar{D}^{*0}\Lambda_c^+)$ processes. By adding the non-resonant amplitudes due to the exchange of \bar{D}^{*0} (\bar{D}^0), we then predict the cross sections of $\gamma p \rightarrow \bar{D}^0\Lambda_c^+(\bar{D}^{*0}\Lambda_c^+)$ for additional experimental tests of the available meson-baryon coupled-channel models of $N_{c\bar{c}}^*$.

PACS numbers: 25.20.Lj, 24.85.+p

I. INTRODUCTION

It is well recognized that the interaction between the nucleon (N) and a $c\bar{c}$ system of charm quark(c) and anti-charm quark(\bar{c}) is mainly due to the gluon-exchange mechanisms. All of the earlier investigations [1–8] have indicated that the $c\bar{c}$ - N interaction is attractive. This implies the possible existence of nuclear systems with hidden charm, as investigated in Refs.[8–10]. For the baryon number $B = 1$ system, it was proposed [11] in 2010 that there exists excited nucleons with $c\bar{c}$ components in the mass range of 4.0 - 5.0 GeV within a meson-baryon coupled-channel model. Such baryons with hidden charm were subsequently also predicted [12–18] as molecular states made of anti-charmed mesons and charmed baryons (such as $\bar{D}^{(*)}\Sigma_c^{(*)}$). Alternatively, they are described as compact pentaquark states made of colored quark clusters [19] or a mixture of the two configurations [20]. The masses from these earlier predictions are qualitatively consistent with the mass (m) and width (Γ) of two Pentaquark states (P_c) identified from analyzing the J/ψ - p invariant mass distributions of the $\Lambda_c^* \rightarrow KJ/\psi p$ decays measured by the LHCb collaboration [21, 22] in 2015. Their results are listed in the left part of Table I.

TABLE I: The masses (m (MeV)) and total widths (Γ (MeV)) of P_c reported in Ref. [21–23]

P_c	2015		P_c	2019	
	m	Γ		m	Γ
$P_c(4380)$	$4380 \pm 8 \pm 29$	$205 \pm 18 \pm 86$	$P_c(4312)$	$4311.9 \pm 0.7^{+6.8}_{-0.6}$	$9.8 \pm 2.7^{+3.7}_{-4.5}$
$P_c(4450)$	$4449.8 \pm 1.7 \pm 2.5$	$39 \pm 5 \pm 19$	$P_c(4440)$	$4440.3 \pm 1.3^{+4.1}_{-4.7}$	$20.6 \pm 4.9^{+8.7}_{-10.1}$
			$P_c(4457)$	$4457.3 \pm 0.6^{+4.1}_{-1.7}$	$6.4 \pm 2.0^{+5.7}_{-1.9}$

The resonance peaks in the J/ψ - p invariant mass distributions from the LHCb measurement [21] had motivated a lot of theoretical efforts [24–67]. Roughly speaking, there are three different interpretations of these peaks:

1. they are due to the excitations of meson-baryon molecular systems which could be made of : (1) anti-charm mesons and charm baryons [24–46], (2) baryons and charmonium [47, 48], (3) the mixture [49, 50] of (1) and (2).
2. they could be the multi-quark states within the conventional constituent quark model [51–53], or the cluster states pictured as a diquark-diquark-antiquark system [54–57] or a diquark-triquark system [58].
3. $P_c(4450)$ may not be a resonance state because it is close to the triangle singularity [59–61] and the observed narrow peak is purely due to kinematic effect, although for some quantum numbers of P_c state preferred in Ref.[21], such as $3/2^-$ or $5/2^+$, the TS can not explain the peak as shown in Ref. [62].

With the the new results from the LHCb collaboration [23], these theoretical interpretations can be better tested. By analyzing the data which are about a factor of 9 more than what they analyzed in 2015, LHCb collaboration obtained three clean peaks which are interpreted as the excitations of three Pentaquark states, as listed in the right part of Table I. Comparing with their results of 2015, the main features of these new data are: (1)

$P_c(4312)$ could be a new Pentaquark state near $\Sigma_c \bar{D}$ threshold. (2) $P_c(4440)$ and $P_c(4457)$ were two narrow states which could not be resolved in their 2015 determination of $P_c(4450)$. (3) $P_c(4380)$ with about 200 MeV width of 2015 could be the very broad state and is not given mass and width in this analysis. It is important to note that these three narrow states are all just below the corresponding anti-charmed meson-charmed baryon threshold and hence the simplest interpretation is that they are made of meson-baryon components, as suggested in Refs.[68–78].

The nucleon resonances with hidden charm, called $N_{c\bar{c}}^*$ from now on in this paper, can also be investigated by using the electromagnetic production of J/ψ from the nucleon, such as $e + p \rightarrow e' + J/\psi + p$ studied in Refs.[11, 12]. The prediction of $\gamma p \rightarrow N_{c\bar{c}}^* \rightarrow J/\psi p$ cross section within the coupled-channel model of Ref. [12] was then made in Ref.[79] by using the Vector Meson Dominance (VMD) Model to generate vector (V) mesons, ρ , ω , and J/ψ , from photon. Few more predictions of $\gamma p \rightarrow N_{c\bar{c}}^* \rightarrow J/\psi p$ had been made [80–85] within the meson-baryon coupled-channel model since 2015. The differences between these works are in their choice of $N_{c\bar{c}}^*$ model, vector mesons included in using VMD, and the background amplitudes which could be calculated from Pomeron-exchange or 2-gluons and 3-gluons exchange model.

In parallel to these theoretical efforts, an experiment [86, 87](JLab(E12-16-007)) on $\gamma p \rightarrow J/\psi p$ near threshold at JLab(E12-16-007) was approved in 2016 and the data from this effort will soon become available. A separate effort at JLab using GlueX detector [88] has recently published [89] their measured total cross sections of $\gamma p \rightarrow J/\psi p$. The main purpose of this work is to provide information for examining whether the $N_{c\bar{c}}^*$ predicted by the available meson-baryon coupled-channel models can be observed in the data from these two experiments.

To proceed, it is necessary to first recognize that P_c states reported by the LHCb collaboration are from the measurements of J/ψ - p invariant mass distribution of the $\Lambda_c \rightarrow K + J/\psi + p$ decay. Thus the information one can use to test the available $N_{c\bar{c}}^*$ models is the total widths and masses of the reported P_c states. The spins and parities of these states can not be determined since a partial-wave analysis of $\Lambda_c \rightarrow K + J/\psi + p$ decays requires detailed angular distribution data, not just the invariant mass distributions. Accordingly, one can not determine the partial decay width for each possible meson-baryon channels of $N_{c\bar{c}}^* \rightarrow J/\psi N, \rho N, \omega N, \bar{D}\Lambda_c, \bar{D}^*\Lambda_c, \bar{D}\Sigma_c, \bar{D}^*\Sigma_c, \dots$. Here we also mention that two of the resonance peaks reported by LHCb collaboration are near the threshold of $\bar{D}^{(*)}\Sigma_c$ channel and thus the identification of resonances in this region must account for the cusp effect in a analysis constrained by the three-body unitarity. The importance of three-body unitarity in analyzing the three-body decays of heavy mesons have been demonstrated [90] recently, but is not considered in the analysis of LHCb collaboration. Therefore, no attempt will be made here to revise the considered meson-baryon models to reproduce the resonance peaks of the LHCb data. Instead, we will only consider the available models which have predicted $N_{c\bar{c}}^*$ with masses within the range of the LHCb data. By using the spins, parities, and partial decay widths from those models, we can then use the VMD to predict the amplitudes of $\gamma p \rightarrow N_{c\bar{c}}^* \rightarrow J/\psi p$. Here we notice that the VMD coupling constant $g_{\gamma,V} = em_V^2/f_V$ for the $\gamma \rightarrow V$ transitions for $V = \rho, \omega, J/\psi$ are conventionally determined from the decay widths of $V \rightarrow \gamma \rightarrow e^+e^-$ with $q^2 = m_V^2$ of the intermediate γ . In the situation of $\gamma p \rightarrow Vp \rightarrow N_{c\bar{c}}^*$, we have $q^2 = 0$, i.e. the intermediate vector is far off-mass-shell, and thus the VMD parameter $g_{\gamma,V}$ must be modified to account for this q^2 -dependence. Ideally, this q^2 -dependence should be calculated from a QCD model as done in Ref.[91]. Here we will

treat it as a phenomenological part of our calculation by introducing a off-shell form factor $F_V = \Lambda^4/(\Lambda^4 + (q^2, m_V^2)^2)$ with Λ determined by the available total cross section data, as will be explained in section III. We also make sure that the parametrization of VMD is gauge invariant when the off-shell form factor is included.

To predict the cross sections of $\gamma p \rightarrow J/\psi p$, it is necessary to include the non-resonant amplitudes due to the gluon-exchange mechanisms. In this work, we use the model of Donnachie and Landshoff [7] within which the gluon-exchange mechanism is phenomenologically parametrized as Pomeron-exchange within the Reggy Phenomenology of high energy reactions. By fitting the total cross section data up to very high energy $W = 300$ GeV, the Pomeron parameters are well determined and can be used to define the non-resonant amplitudes in the near threshold region of our interest in this paper. Our approach is therefore different from the approaches using the models of two-gluon and three-gluon exchange of Refs.[92], as will be discussed later.

For additional studies of $N_{c\bar{c}}^*$ excitations, we have also explored other meson photo-production processes which do not have Pomeron-exchange mechanisms. We have found that experiments on $\gamma p \rightarrow \bar{D}^0 \Lambda_c^+ (\bar{D}^{*0} \Lambda_c^+)$ could be useful. With the same VMD model and the same coupled-channel models of $N_{c\bar{c}}^*$, we have calculated the resonant amplitudes for the $\gamma p \rightarrow V p \rightarrow N_{c\bar{c}}^* \rightarrow \bar{D}^0 \Lambda_c^+ (\bar{D}^{*0} \Lambda_c^+)$ processes. By adding the non-resonant amplitudes due to the exchange of \bar{D}^{*0} (\bar{D}^0), we then predict the cross sections of $\gamma p \rightarrow \bar{D}^0 \Lambda_c^+ (\bar{D}^{*0} \Lambda_c^+)$ for additional experimental tests of the available meson-baryon coupled-channel models of $N_{c\bar{c}}^*$.

The paper is organized as follows. In section II, we give formulas for calculating the cross sections of $\gamma p \rightarrow J/\psi p$, and present formula for calculating the Pomeron-exchange amplitude and the $\gamma p \rightarrow N_{c\bar{c}}^* \rightarrow J/\psi p$ resonant amplitudes. In section III, we present our results for $\gamma p \rightarrow J/\psi p$. The results for $\gamma p \rightarrow \bar{D}^0 \Lambda_c, \bar{D}^{*0} \Lambda_c$ are given in section IV. The discussion and summary will be given in the last section.

II. CROSS SECTION FORMULA FOR VECTOR MESON PHOTO-PRODUCTION REACTION ON THE NUCLEON

We consider the photo-production of a Meson (M)-Baryon (B) system : $\gamma(q) + p(p) \rightarrow M(q') + B(p')$. In the center of mass system, the four-momentum of these particles can be defined as

$$\begin{aligned} q &= (k, \vec{k}) \\ q' &= (E_M(k'), \vec{k}') \\ p &= (E_N(k), -\vec{k}) \\ p' &= (E_B(k), -\vec{k}') \\ P &= q + q' = p + p' = (W, \vec{0}), \end{aligned}$$

where $k(k')$ is the length of three momenta $\vec{k}(\vec{k}')$, $E_a(k) = \sqrt{m_a^2 + k^2}$ is the energy of a particle with mass m_a , and W is the invariant mass of system. For a given W and angle (Ω) between \vec{k} and \vec{k}' , all of the above kinematic variables are determined by $W = k + E_N(k) = E_M(k') + E_B(k')$. The differential cross section can then be written

$$\frac{d\sigma}{d\Omega} = \frac{(2\pi)^4}{k^2} \rho_{\gamma N}(k) \rho_{MB}(k') \frac{1}{4} \sum_{\lambda_\gamma, \lambda_M} \sum_{m_s, m'_s} | \langle \vec{k}' \chi_{M m'_s} | T(W) | \vec{k} \chi_{\gamma m_s} \rangle |^2, \quad (1)$$

where λ'_M (λ_γ) is the helicity of the meson M (photon γ), m_s (m'_s) is the z-component of the spin of initial proton p (final baryon B). The phase space factors in Eq.(1) are

$$\begin{aligned}\rho_{\gamma N}(k) &= \frac{k^2 E_N(k)}{W} \\ \rho_{MB}(k') &= \frac{k' E_M(k') E_N(k')}{W}\end{aligned}\quad (2)$$

The reaction amplitude is written as

$$\langle \vec{k}' \lambda'_M m'_s | T(W) | \vec{k} \lambda_\gamma m_s \rangle = \frac{1}{(2\pi)^3} \sqrt{\frac{m_N m_B}{4k E_N(k) E_M(k') E_B(k')}} \epsilon_\nu(q, \lambda_\gamma) [j^\nu_{\lambda'_M, m'_s, m_s}(q', p', q, p)] \quad (3)$$

where $\epsilon_\nu(q, \lambda_\gamma)$ is the polarization vector of photon, and $j^\nu_{\lambda'_M, m'_s, m_s}(q, p, q', p')$ is a Lorentz covariant current matrix element. For the vector meson photo-production $\gamma p \rightarrow J/\psi p$ ($M = J/\psi$ and $B = N$) process, the current matrix element can be written as

$$j^\nu_{\lambda'_{J/\psi}, m'_s, m_s}(q, p, q', p') = \bar{u}_p(p', m'_s) \epsilon_\mu^*(q', \lambda'_{J/\psi}) \mathcal{M}^{\mu\nu}(q, p, q', p') u_p(p, m_s), \quad (4)$$

where $u_a(p, m_s)$ is the spinor of the baryon a (with the normalization $\bar{u}_a(p, m_s) u_a(p, m'_s) = \delta_{m_s, m'_s}$), $\epsilon_\nu(q, \lambda'_{J/\psi})$ is the polarization vector of J/ψ . The current matrix element must satisfy the gauge invariance condition $j^\nu q_\nu = 0$.

In this work, we assume that the J/ψ photo-production amplitudes $\mathcal{M}^{\mu\nu}(q, p, q', p')$ of Eq.(4) can be written as

$$\mathcal{M}^{\mu\nu}(q, p, q', p') = \mathcal{M}_{\mathbb{P}}^{\mu\nu}(q, p, q', p') + \mathcal{M}_{N^*}^{\mu\nu}(q, p, q', p') \quad (5)$$

where $\mathcal{M}_{\mathbb{P}}^{\mu\nu}(q, p, q', p')$ is the Pomeron-exchange amplitude of Donnachie and Landshoff, and $\mathcal{M}_{N^*}^{\mu\nu}(q, p, q', p')$ is the $\gamma N \rightarrow N_{cc}^* \rightarrow J/\psi N$ amplitude. In the following, we will describe the calculations of these two amplitudes.

A. Pomeron-exchange mechanism

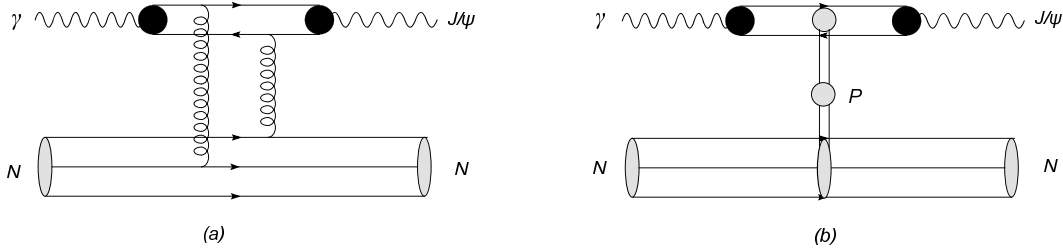


FIG. 1: Gluon-exchange mechanism of $\gamma N \rightarrow J/\psi + N$

It is well recognized that the photo-production of J/ψ from the nucleon is mainly due to gluon-exchange mechanism, such as the leading two-gluon exchange mechanism illustrated in

Fig.1 (a). It is also known that Pomeron-exchange has been an essential element in Reggy Phenomenology. Within the model of Donnachie and Landshoff (DL) [7], it is assumed that Pomeron (\mathbb{P}) can be identified with gluons and the Pomeron-exchange mechanism can be parametrized in terms of Pomeron-quark coupling constant β_q and appropriately form factors at the $\mathbb{P} J/\psi \rightarrow J/\psi$ and $\mathbb{P} N \rightarrow N$ vertices. The DL model is illustrated in Fig.1 (b). Following a study of non perturbative two-gluon exchanges [93], they further assume the Pomeron-Photon analogy that the Pomeron can be treated as a $C = +1$ isoscalar photon to parametrize the quark-Pomeron vertex. Thus the $\mathbb{P} N \rightarrow N$ vertex can be expressed in term of the isoscalar electromagnetic form factor of the nucleon. Following Ref. [94], the Pomeron-exchange amplitude in Eq.(5) is written as:

$$\mathcal{M}_{\mathbb{P}}^{\mu\nu}(q, p, q', p') = G_{\mathbb{P}}(s, t) \mathcal{T}_{\mathbb{P}}^{\mu\nu}(q, p, q', p') \quad (6)$$

with

$$\mathcal{T}_{\mathbb{P}}^{\mu\nu}(q, p, q', p') = i12 \frac{eM_V^2}{f_V} \beta_{q_V} F_V(t) \beta_{u/d} F_1(t) [\not{q} g^{\mu\nu} - q^\mu \gamma^\nu], \quad (7)$$

where β_{q_V} ($\beta_{u/d}$) defines the coupling of the Pomeron with the quark q_V (u or d) in the vector meson V (nucleon N). Here we have introduced the form factor for the Pomeron-vector meson vertex as

$$F_V(t) = \frac{1}{M_V^2 - t} \left(\frac{2\mu_0^2}{2\mu_0^2 + M_V^2 - t} \right) \quad (8)$$

where $t = (p - p')^2$. By using the Pomeron-photon analogy mentioned above, the form factor for the Pomeron-nucleon vertex is defined by the isoscalar electromagnetic form factor of the nucleon as

$$F_1(t) = \frac{4M_N^2 - 2.8t}{(4M_N^2 - t)(1 - t/0.71)^2}. \quad (9)$$

Here t is in unit of GeV^2 , and M_N is the proton mass. Note that the factor $\frac{eM_V^2}{f_V}$ in Eq.(7) implies a relation between the DL model and the VMD.

The crucial ingredient of the Reggy Phenomenology is the propagator $G_{\mathbb{P}}$ for the Pomeron in Eq.(6). It is of the following form :

$$G_{\mathbb{P}} = \left(\frac{s}{s_0} \right)^{\alpha_P(t)-1} \exp \left\{ -\frac{i\pi}{2} [\alpha_P(t) - 1] \right\}, \quad (10)$$

where $s = (q + p)^2 = W^2$, $\alpha_P(t) = \alpha_0 + \alpha'_P t$. By fitting the data of ρ^0 , ω , and ϕ photo-production[94], the parameters of the model have been determined: $\mu_0 = 1.1 \text{ GeV}^2$, $\beta_{u/d} = 2.07 \text{ GeV}^{-1}$, $\beta_s = 1.6 \text{ GeV}^{-1}$, $\alpha_0 = 1.08$ and $\alpha'_P = 1/s_0 = 0.25 \text{ GeV}^{-2}$. In our previous paper [9], we found that with the same μ_0^2 , $\beta_{u/d}$, and α'_P , the J/ψ photo-production data can be fitted by setting $\beta_c = 0.84 \text{ GeV}^{-1}$ and choosing a larger $\alpha_0 = 1.25$. In the left side of Fig.2, the results (black solid curves) from the constructed Pomeron-exchange model are compared with all of the the total cross section data of $\gamma p \rightarrow J/\psi p$ up to invariant mass $W = 300 \text{ GeV}$. Here we note that the two-gluon (dotted curves) and three-gluon (dot-dashed curves) exchange models, with the parameters given in Refs.[92] can not describe the data above about $W = 10 \text{ GeV}$. The new data from JLab GlueX collaboration are considerably

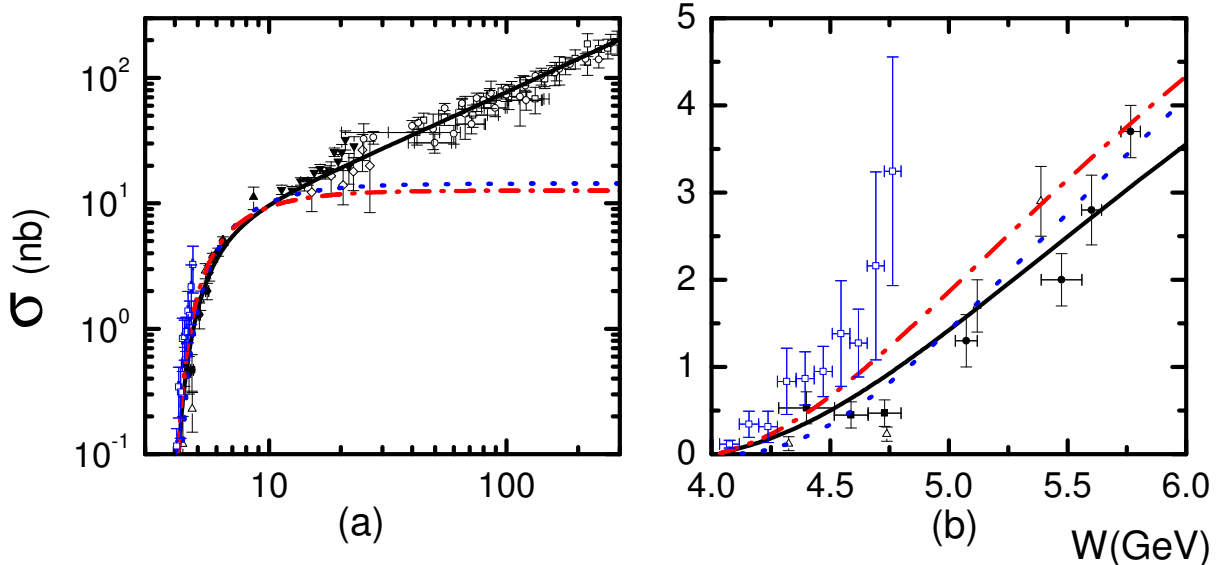


FIG. 2: Total cross sections of photo-production of J/ψ on the proton target. The solid curve is from the DL model of Pomeron-exchange. The dotted (dash-dotted) curves are from the 2-gluon exchange (2-gluon+3 gluon-exchange) models. The experimental data can be found in Ref. [9], except blue open spares are from Ref. [88]

larger in magnitudes than the previous data, as can be seen more clearly in the right side of Fig.2. While these data can be better described by the 2g+3g exchange model, as also shown by the GlueX collaboration, they need further confirmation from separate experiments at JLab. Thus our study of $N_{c\bar{c}}^*$ starts with Fig.3 in which the data before 2018 are compared with the results calculated from using the Pomeron-exchange model.

B. Excitation of $N_{c\bar{c}}^*$ resonances

We focus on the $N_{c\bar{c}}^*$ predicted by the meson-baryon coupled-channel models with the parameters constrained by the SU(4) symmetry and the fit to the meson-baryon reaction data. Alternatively, $N_{c\bar{c}}^*$ can be predicted by constituent quark models or non-perturbative QCD models. These are however not considered in this work.

In Table II, we list the predictions from most, if not all, of the coupled-channel models of $N_{c\bar{c}}^*$ in the literatures. The relative importance of the predicted $N_{c\bar{c}}^*$ in determining $\gamma p \rightarrow J/\psi p$ can be estimated by using a well known relation between the total cross section $\sigma^{(tot)}$ at resonance energy $W = M_R$ and the partial decay widths $\Gamma_{N_{c\bar{c}}^*, J/\psi p}$ of $N_{c\bar{c}}^* \rightarrow J/\psi p$, $\Gamma_{N_{c\bar{c}}^*, \gamma p}$ of $N_{c\bar{c}}^* \rightarrow \gamma p$, and the total width $\Gamma_{N_{c\bar{c}}^*}^{(tot)}$:

$$\sigma^{(tot)}(W = M_R) = \frac{2J + 1}{4} \frac{4\pi}{q_R^2} \frac{\Gamma_{N_{c\bar{c}}^*, J/\psi p} \Gamma_{N_{c\bar{c}}^*, \gamma p}}{[\Gamma_{N_{c\bar{c}}^*}^{(tot)}]^2} \quad (11)$$

where J is the spin of $N_{c\bar{c}}^*$, and q_R is defined by the resonance mass by $M_R = \sqrt{M_N^2 + q_R^2} + q_R$. We note here that except the model by Lin et al[45] the decay width $\Gamma_{N_{c\bar{c}}^*, \gamma p}$ to the γp channel are not predicted by the models listed in Table II. Thus the only way we can use these

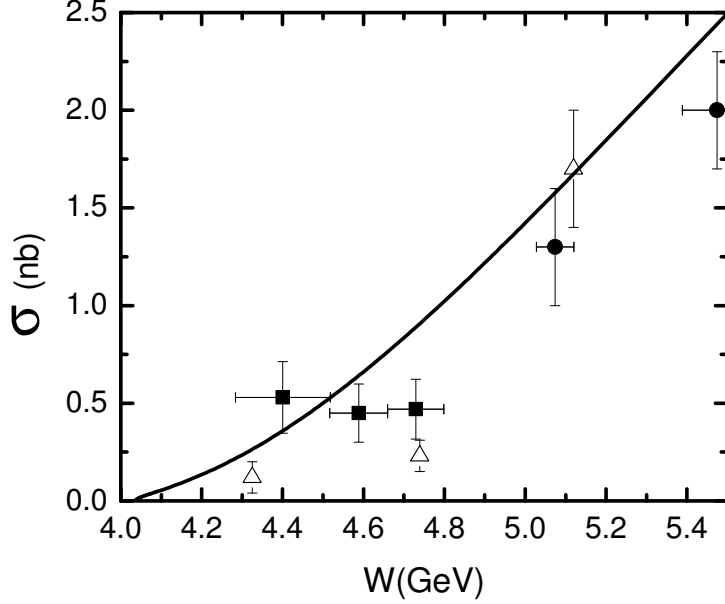


FIG. 3: The total cross section of $\gamma p \rightarrow J/\psi + p$ via Pomeron-exchange with the center mass energy W in the near threshold energy region. The experimental data are from Ref. [95–97]

models is to use the VMD model to describe the excitation of $N_{c\bar{c}}^*$ as the $\gamma N \rightarrow V N \rightarrow N_{c\bar{c}}^*$ mechanism with $V = \rho, \omega, J/\psi$, as illustrated in Fig.4.

In Table II, we also see that the predicted $N_{c\bar{c}}^*$ mainly decay into channels associated with the \bar{D} meson and charmed Σ_c baryons, as specified as "Main Channel" in the table. However, the available energy at JLab is not high enough to investigate the $\gamma p \rightarrow \bar{D}\Sigma_c$ process. Instead the experiment on the process $\gamma p \rightarrow \bar{D}\Lambda_c$ may be possible. Thus we will also consider the $\gamma p \rightarrow \bar{D}\Lambda_c$ reaction which does not have Pomeron-exchange mechanism. This can be studied using the models which also provide partial decay widths of $N_{c\bar{c}}^* \rightarrow \bar{D}\Lambda_c$, as also shown in Table II.

To proceed, we recall that the VMD is defined by the following Lagrangian:

$$L_{VMD}(x) = \frac{em_V^2}{f_V} A_\mu(x) \phi_V^\mu(x) \quad (12)$$

where m_V is the mass of the vector meson V , A_μ and ϕ_V^μ are the field operators for the photon and vector meson, respectively. The width of $V \rightarrow e^+e^-$ can then be calculated by

$$\Gamma_{V \rightarrow e^+e^-} = \frac{1}{3} \alpha^2 m_V \frac{4\pi}{f_V^2} \quad (13)$$

By using the data of $\Gamma_{V \rightarrow e^+e^-}$, the decay constants of Eq.(12) can be determined : $f_\rho = 5.33$, $f_\omega = 15.2$, $f_\phi = 13.4$, and $f_{J/\psi} = 11.2$. For our later discussions, we here note that these coupling constants are determined at the photon four-momentum $q^2 = m_V^2$. Thus the use of the Lagrangian Eq.(12) in other processes with real photon $q^2 = 0$, a model must be used to account for the off-shell effects on these coupling constant. In our calculations, we thus

will set

$$\frac{1}{f_V} \rightarrow \frac{1}{f_V} F_V(q^2) \quad (14)$$

$$F_V(m_V^2) = 1 \quad (15)$$

Ideally $F_V(q^2)$ should be calculated from the quark-loop mechanism $V \rightarrow q\bar{q} \rightarrow \gamma(q^2)$ within a non-perturbative QCD model. Here, we will determine it phenomenologically, as will be specified later.

With VMD, the $\gamma N \rightarrow N_{c\bar{c}}^*$ amplitude can be calculated from $\gamma N \rightarrow V_{VMD} N \rightarrow N_{c\bar{c}}^*$, where $V_{VMD} = \rho, \omega, J/\psi$ and $V_{VMD} N \rightarrow N_{c\bar{c}}^*$ calculated from the considered meson-baryon coupled-channel models of $N_{c\bar{c}}^*$. The full amplitude $\gamma N \rightarrow N_{c\bar{c}}^* \rightarrow V N$ can then be calculated from by using $N_{c\bar{c}}^* \rightarrow V N$ generated from the same coupled-channel models of $N_{c\bar{c}}^*$. In the following subsections, we will give formula for calculating these amplitudes. With the calculated $\Gamma_{N_{c\bar{c}}^*, \gamma p}$ and the predicted widths $\Gamma_{N_{c\bar{c}}^*, J/\psi p}$ and $\Gamma_{N_{c\bar{c}}^*}^{(tot)}$ listed in Table II, we then can use Eq.(11) to estimate the predicted $\sigma^{(tot)}$ for each model and then select only the cases that the estimated $\sigma^{(tot)}$ are close to the available data to make predictions.

TABLE II: The mass (m (MeV)), total width (Γ (MeV), for $\Gamma_{p\gamma}$ (kev)), branch decay width (Γ) of $J/\psi N$, ρN , ωN , $\bar{D}\Lambda_c$ and $\bar{D}^*\Lambda_c$ are listed with various models. The No. 17 and 18 are from the experimental data. In Ref. [42], the mass is used from experimental data. Others are all calculated from models.

No.	J^P	m	Γ	$\Gamma_{J/\psi N}$	$\Gamma_{\rho N}$	$\Gamma_{\omega N}$	$\Gamma_{\bar{D}\Lambda_c}$	$\Gamma_{\bar{D}^*\Lambda_c}$	$\Gamma_{p\gamma}$	MC	Ref.
1	$\frac{1}{2}^-$	4262	35.6	10.3	—	—	0.01	—	—	$\bar{D}\Sigma_c$	[17]
2		4308	7.1	1.2	—	—	0.02	1.4	—	$\bar{D}\Sigma_c$	[98]
3		4412	47.3	19.2	3.2	10.4	—	—	—	$\bar{D}^*\Sigma_c$	[11, 12]
4		4410	58.9	52.5	—	—	0.8	0.7	—	$\bar{D}^*\Sigma_c$	[17]
5		4460	6.2	3.9	—	—	1.0	0.3	—	$\bar{D}^*\Sigma_c$	[98]
6		4481	57.8	14.3	—	—	1.02	0.3	—	$\bar{D}^*\Sigma_c^*$	[17]
7	$\frac{3}{2}^-$	4334	38.8	38.0	—	—	—	0.8	—	$\bar{D}\Sigma_c^*$	[17]
8		4375	2.4	1.5	—	—	—	0.9	—	$\bar{D}\Sigma_c^*$	[98]
9		4380	144.3	3.8	1.4	5.3	1.2	131.3	0.7	$\bar{D}\Sigma_c^*$	[42]
10		4380	69.9	16.6	0.15	0.6	17.0	35.3	—	$\bar{D}^*\Sigma_c$	[42]
11		4412	47.3	19.2	3.2	10.4	—	—	—	$\bar{D}^*\Sigma_c$	[11, 12]
12		4417	8.2	4.6	—	—	—	3.1	—	$\bar{D}^*\Sigma_c$	[17]
13		4450	139.8	16.3	0.14	0.5	41.4	72.3	—	$\bar{D}^*\Sigma_c$	[42]
14		4450	21.7	0.03	—	—	1.4	6.8	—	$\bar{D}^*\Sigma_c$	[48]
15		4450	16.2	11	—	—	0.6	4.2	—	$\Psi'N$	[48]
16		4453	1.8	1.5	—	—	—	0.3	—	$\bar{D}\Sigma_c^*$	[98]
17		4481	34.7	32.8	—	—	—	1.2	—	$\bar{D}^*\Sigma_c^*$	[17]
18	$\frac{5}{2}^+$	4450	46.4	4.0	0.3	0.3	18.8	20.5	1.13	$\bar{D}^*\Sigma_c$	[42]
19	$\frac{3}{2}^-, \frac{5}{2}^+$	$4380_{\pm 29}^{\pm 8}$	$205_{\pm 86}^{\pm 18}$	—	—	—	—	—	—	Exp	[21, 22]
20		$4450_{\pm 3}^{\pm 2}$	$39_{\pm 19}^{\pm 5}$	—	—	—	—	—	—	Exp	[21, 22]

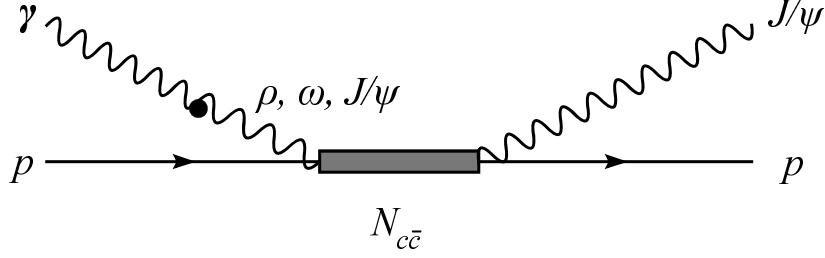


FIG. 4: The diagram for $\gamma p \rightarrow N_{c\bar{c}} \rightarrow J/\psi p$ with the VMD by ρ , ω and J/ψ coupled with γ .

1. The $N_{c\bar{c}}^* \rightarrow NV$ transition amplitudes

Following the formulation of Ref.[99, 100], the $N_{c\bar{c}}^*(J^P, P) \rightarrow N(p_N) + V(p_V)$ transitions for spin-parity $J^P = \frac{1}{2}^-, \frac{3}{2}^-,$ and $\frac{5}{2}^+$ can be written as

$$\mathcal{M}_{N_{c\bar{c}}^*(\frac{1}{2}^-)NV}(P; p_V p_N) = \bar{u}_N(p_N) \gamma_5 \tilde{\gamma}_\mu u_{N^*}(P) \epsilon_\nu^*(p_V) \left(g_{1V} g^{\mu\nu} - f_{1V} \left(\frac{3}{2} \frac{\tilde{r}^\mu \tilde{r}^\nu}{\tilde{r}^2} - \frac{1}{2} \tilde{g}_{N^*}^{\mu\nu} \right) \right) \quad (16)$$

$$\begin{aligned} \mathcal{M}_{N_{c\bar{c}}^*(\frac{3}{2}^-)NV}(P; p_V p_N) &= \bar{u}_N(p_N) u_{N^* \mu}(P) \epsilon_\nu^*(p_V) \left(g_{3V} g^{\mu\nu} - f_{3V} \left(\frac{3}{2} \frac{\tilde{r}^\mu \tilde{r}^\nu}{\tilde{r}^2} - \frac{1}{2} \tilde{g}_{N^*}^{\mu\nu} \right) \right) \\ &+ h_{3V} \epsilon_{\mu\nu\lambda\delta} \bar{u}_N \gamma_5 (\tilde{\gamma}^\mu g_\alpha^\beta + \tilde{\gamma}_\alpha g^{\mu\beta}) u_{N^* \beta} \epsilon_\nu^* \left(\frac{\tilde{r}^\alpha \tilde{r}^\lambda}{\tilde{r}^2} - \frac{1}{3} \tilde{g}_{N^*}^{\alpha\lambda} \right) \hat{P}^\delta, \end{aligned} \quad (17)$$

$$\begin{aligned} \mathcal{M}_{N_{c\bar{c}}^*(\frac{5}{2}^+)NV}(P; p_V p_N) &= \bar{u}_N(p_N) u_{N^* \mu\nu}(P) \epsilon_\alpha^*(p_V) \\ &\times \left(\frac{g_{5V}}{m_N} g^{\alpha\mu} \tilde{r}^\nu - \frac{f_{5V}}{m_N} \left(\frac{5}{3} \frac{\tilde{r}^\mu \tilde{r}^\nu \tilde{r}^\alpha}{\tilde{r}^2} - \frac{1}{3} (\tilde{g}_{N^*}^{\mu\nu} \tilde{r}^\alpha + \tilde{g}_{N^*}^{\nu\alpha} \tilde{r}^\mu + \tilde{g}_{N^*}^{\alpha\mu} \tilde{r}^\nu) \right) \right) \\ &+ \frac{h_{5V}}{m_N} \epsilon_{\mu\nu\lambda\delta} \bar{u}_N \gamma_5 (\tilde{\gamma}^\mu g_{\xi\alpha} g_{\sigma\beta} + \tilde{\gamma}_\xi g_{\sigma\beta} g_{\mu\beta} + \tilde{\gamma}_\sigma g_{\mu\beta} g_{\xi\beta}) u_{N^*}^{\alpha\beta} \epsilon_\nu^* \\ &\times \left(\frac{\tilde{r}^\xi \tilde{r}^\lambda \tilde{r}^\sigma}{\tilde{r}^2} - \frac{1}{3} (\tilde{g}_{N^*}^{\xi\sigma} \tilde{r}^\lambda + \tilde{g}_{N^*}^{\sigma\lambda} \tilde{r}^\xi + \tilde{g}_{N^*}^{\lambda\xi} \tilde{r}^\sigma) \right) \hat{P}^\delta, \end{aligned} \quad (18)$$

where

$$r^\mu = p_N^\mu - p_V^\mu, \quad \tilde{g}_{N^*}^{\mu\nu} = g^{\mu\nu} - \frac{P^\mu P^\nu}{W^2}, \quad (19)$$

$$\tilde{r}^\nu = r_\mu \tilde{g}_{N^*}^{\mu\nu}, \quad \tilde{\gamma}^\nu = \gamma_\mu \tilde{g}_{N^*}^{\mu\nu}, \quad (20)$$

$$\hat{P}_\mu = P_\mu / W \quad (21)$$

The terms with coupling constants f_{2JV} and h_{2JV} term are the contributions from higher partial waves. For simplicity, we neglect these terms and set $f_{2JV} = h_{2JV} = 0$. We thus can use the partial decay width $\Gamma_{N_{c\bar{c}}^*NV}$ listed in Table II to determine the parameter g_{2JV} by the following formula:

$$\Gamma_{N_{c\bar{c}}^*NV} = \frac{|p|}{8\pi m_{N_{c\bar{c}}^*}^2} |\mathcal{M}_{N_{c\bar{c}}^*NV}|^2, \quad (22)$$

where $|p\rangle$ is on-shell momentum of final state vector in the rest frame of $N_{c\bar{c}}^*$.

The determined g_{2JV} for $V = J/\psi$ are listed in the 5th column of Table III.

TABLE III: coupling constants g_V and \tilde{g}_V determined from fitting the partial decay widths listed in Table II. $\Gamma_{\gamma p}$ are partial decay widths calculated from \tilde{g}_V within VMD, as explained in the text. $\sigma^{(tot)}$ is the total cross section of $\gamma p \rightarrow J/\psi p$ calculated from using Eq.(20) by choosing $\Lambda = 0.55$ GeV for the off-shell form factor $F_V(q^2)$.

No.	J^P	m	Γ_{tot}	g_{2JV} $J/\psi p$	\tilde{g}_{2JV} $J/\psi p$	\tilde{g}_{2JV} ρp	\tilde{g}_{2JV} ωp	$\Gamma_{p\gamma}$ (keV)	$\sigma^{(tot)}$ (nb)
1	$\frac{1}{2}^-$	4262	35.6	0.39	0.32	—	—	3.9×10^{-5}	1.9×10^{-4}
2		4308	7.1	0.13	0.11	—	—	4.5×10^{-6}	5.9×10^{-9}
3		4412	47.3	0.46	0.38	0.078	0.14	1.14	5.4
4		4410	58.9	0.75	0.62	—	—	1.5×10^{-4}	1.3×10^{-3}
5		4460	6.2	0.20	0.16	—	—	1.1×10^{-5}	6.2×10^{-4}
6		4481	57.8	0.37	0.31	—	—	3.8×10^{-5}	8.8×10^{-5}
7	$\frac{3}{2}^-$	4334	38.8	1.19	0.98	—	—	1.3×10^{-4}	3.7×10^{-3}
8		4375	2.4	0.23	0.19	—	—	4.6×10^{-6}	1.4×10^{-3}
9		4380	144.3	0.36	0.30	0.090	0.17	0.53	0.11
10		4380	69.9	0.75	0.62	0.039	0.059	0.060	0.23
11		4412	47.3	0.79	0.65	0.14	0.24	1.1	10.8
12		4417	8.2	0.39	0.32	—	—	1.4×10^{-5}	1.0×10^{-3}
13		4450	139.8	0.71	0.58	0.028	0.053	0.054	0.048
14		4450	21.7	0.030	0.025	—	—	8.4×10^{-8}	5.8×10^{-9}
15		4450	16.2	0.58	0.48	—	—	3.1×10^{-5}	1.4×10^{-3}
16		4453	1.8	0.21	0.18	—	—	4.2×10^{-6}	2.2×10^{-3}
17		4481	34.7	0.98	0.81	—	—	8.8×10^{-5}	2.6×10^{-3}
18	$\frac{5}{2}^+$	4450	46.4	0.35	0.27	0.016	0.016	8.3×10^{-2}	0.25

2. The $N_{c\bar{c}}^* \rightarrow N\gamma$ transition amplitudes

As illustrated in Fig.4, we assume that the $N_{c\bar{c}}^* \rightarrow N\gamma$ transition amplitudes can be calculated by the $\gamma \rightarrow V$ transition defined by the VMD Lagrangian Eq.(12), the propagator of V , and the $VN \rightarrow N_{c\bar{c}}^*$ amplitudes defined in Eqs.(16)-(21). Since we can determine the parameters by using only one value of $\Gamma_{N_{c\bar{c}}^*, \gamma N}$ predicted by a $N_{c\bar{c}}^*$ model, we need to make simplification. Here we also need to make sure that the simplified amplitudes are gauge invariant. We find that this can be accomplished by setting $h_{2JV} = 0$ like what we have chosen in determining $\Gamma_{N_{c\bar{c}}^* \rightarrow NV}$, but we need to keep the f_{2JV} term and set $g_{2JV} = f_{2JV} = \tilde{g}_{2JV}$. For example, the amplitude of $N^*(\frac{1}{2}^-) \rightarrow N\rho \rightarrow N\gamma$ with the simplification $h_{2JV} = 0$ is:

$$\mathcal{M}_{N^*(\frac{1}{2}^-) \rightarrow N\rho \rightarrow N\gamma}(P; q = p_\rho p_N) = \frac{ie}{f_\rho} \frac{-m_\rho^2}{q^2 - m_\rho^2 + i\Gamma_\rho m_\rho} \mathcal{M}^\nu(P; p_\rho p_N) \epsilon_\gamma^{*\nu}(q) \quad (23)$$

with

$$\mathcal{M}^\nu(P; q = p_\rho p_N) = \bar{u}_{N^*}(P) \gamma_5 \tilde{\gamma}_\mu u_N(p_N) \left(g_{1\rho} g^{\mu\nu} - f_{1\rho} \left(\frac{3 \tilde{r}^\mu \tilde{r}^\nu}{2 \tilde{r}^2} - \frac{1}{2} \tilde{g}_{N^*}^{\mu\nu} \right) \right) \tilde{g}_{\rho \nu}{}^\nu(q) \quad (24)$$

Obviously this amplitude will be gauge invariant if $\mathcal{M}^\nu q_\nu = 0$. However it is straightforward to show that $\mathcal{M}^\nu q_\nu \sim (g_{1\rho} - f_{1\rho}) \neq 0$. Therefore a simple way to have a gauge invariant amplitude is to set $g_{2JV} = f_{2JV} = \tilde{g}_{2JV}$. This is part of phenomenology and need to be improved in future. For our present limited and exploratory purpose, this simplification is sufficient.

By using Eqs.(16)-(18) and setting $g_{2JV} = f_{2JV} = \tilde{g}_{2JV}$ and $h_{2JV} = 0$, we can then use Eq.(22) to determine \tilde{g}_{2JV} by using the partial decay widths listed in Table II. The resulting \tilde{g}_{2JV} are listed in the 6th-8th columns of Table III. Including the off-shell form factor $F_V(q^2)$ according to Eq.(14), we then get the following expressions for the $N_{c\bar{c}}^* \rightarrow VN \rightarrow \gamma N$ transition amplitudes:

$$\begin{aligned} \mathcal{M}_{N^*(\frac{1}{2}^-) \rightarrow NV \rightarrow N\gamma}(P; q p_N) &= \frac{ie}{f_V - m_V^2 + i\Gamma_V m_V} \frac{-m_V^2 \tilde{g}_{1V}}{\tilde{g}_{1V}} \bar{u}_N(p_N) \gamma_5 \tilde{\gamma}_\mu u_{N^*}(P) \\ &\times [\epsilon_{\gamma \nu}^* \left(g^{\mu\nu} - \frac{3 \tilde{r}^\mu \tilde{r}^\nu}{2 \tilde{r}^2} + \frac{1}{2} \tilde{g}_{N^*}^{\mu\nu} \right) F_V(q^2)], \end{aligned} \quad (25)$$

$$\begin{aligned} \mathcal{M}_{N^*(\frac{3}{2}^-) \rightarrow NV \rightarrow N\gamma}(P; q p_N) &= \frac{ie}{f_V - m_V^2 + i\Gamma_V m_V} \frac{-m_V^2 \tilde{g}_{3V}}{\tilde{g}_{3V}} \bar{u}_N(p_N) u_{N^* \mu}(P) \\ &\times [\epsilon_{\gamma \nu}^* \left(g^{\mu\nu} - \frac{3 \tilde{r}^\mu \tilde{r}^\nu}{2 \tilde{r}^2} + \frac{1}{2} \tilde{g}_{N^*}^{\mu\nu} \right) F_V(q^2)], \end{aligned} \quad (26)$$

$$\begin{aligned} \mathcal{M}_{N^*(\frac{5}{2}^+) \rightarrow NV \rightarrow N\gamma}(P; q p_N) &= \frac{ie}{f_V - m_V^2 + i\Gamma_V m_V} \frac{-m_V^2 \tilde{g}_{5V}/m_N}{\tilde{g}_{5V}} \bar{u}_N(p_N) u_{N^* \mu\nu}(P) \epsilon_{\gamma \alpha}^* F_V(q^2) \\ &\times \left(g^{\alpha\mu} \tilde{r}^\nu - \frac{5 \tilde{r}^\mu \tilde{r}^\nu \tilde{r}^\alpha}{3 \tilde{r}^2} + \frac{1}{3} (\tilde{g}_{N^*}^{\mu\nu} \tilde{r}^\alpha + \tilde{g}_{N^*}^{\nu\alpha} \tilde{r}^\mu + \tilde{g}_{N^*}^{\alpha\mu} \tilde{r}^\nu) \right). \end{aligned} \quad (27)$$

where $p_V = q$ is used to evaluate \tilde{r}^ν and $\tilde{g}_{N^*}^{\alpha\mu}$ according to Eqs.(19)-(20). For the off-shell form factors, we assume

$$F_V(q) = \frac{\Lambda_V^4}{\Lambda_V^4 + (q^2 - m_V^2)^2}. \quad (28)$$

With the determined \tilde{g}_V listed in Table III and a given choice of the cut off Λ_V , we can use the $N^* \rightarrow NV \rightarrow N\gamma$ amplitudes given in Eqs.(25)-(27) to calculate the decay width of $N^* \rightarrow N\gamma$ within VMD :

$$\Gamma_{N^* \rightarrow N\gamma} = \frac{1}{8\pi} \frac{k}{m_{N^*}^2} \left| \sum_V M_{N^* \rightarrow NV \rightarrow N\gamma} \right|^2. \quad (29)$$

The cut-off Λ is a parameter of the model. In Table III we list the calculated $\Gamma_{N^* \rightarrow N\gamma}$ for each model by setting $\Lambda = 0.55$ GeV (The dependence on the value of Λ will be discussed in the next section). By using the partial decay widths listed in Tables II and III we can use Eq.(11) to estimate the total cross section $\sigma^{(tot)}$ of $\gamma p \rightarrow J/\psi p$ at the resonance positions, as also given in the 9th column of Table III.

3. The amplitude of $\gamma p \rightarrow N_{c\bar{c}}^* \rightarrow J/\psi p$

The amplitude $\gamma p \rightarrow N_{c\bar{c}}^* \rightarrow J/\psi p$ is shown in Fig.4. By using the definition of vertexes of $N^* \rightarrow NV$ as shown Eq.(16-18) and $N^* \rightarrow N\gamma$ as shown Eq.(25-27), we can write the amplitude $\mathcal{M}_{N^*}^{\mu\nu}(q, p, q', p')$ which defined in Eq.(4):

$$\begin{aligned} \mathcal{M}_{N^*(\frac{1}{2}^-)}^{\mu\nu}(q, p, q', p') &= \sum_{V=J/\psi, \rho, \omega} g_{1J/\psi} \gamma_5 \tilde{\gamma}_\alpha \tilde{g}^{\alpha\mu}(q) \frac{\not{q} + \not{p} + m_{N_{c\bar{c}}^*}}{W^2 - m_{N_{c\bar{c}}^*}^2 + i\Gamma_{N_{c\bar{c}}^*} m_{N_{c\bar{c}}^*}} F_V(0) \\ &\times \frac{ie}{f_V - m_V^2 + i\Gamma_V m_V} \frac{-m_V^2 \tilde{g}_{1V}}{m_V} \gamma_5 \tilde{\gamma}_\beta \left(g^{\beta\nu} - \frac{3}{2} \frac{\tilde{r}^\beta \tilde{r}^\nu}{\tilde{r}^2} + \frac{1}{2} \tilde{g}_{N^*}^{\beta\nu} \right), \end{aligned} \quad (30)$$

$$\begin{aligned} \mathcal{M}_{N^*(\frac{3}{2}^-)}^{\mu\nu}(q, p, q', p') &= \sum_{V=J/\psi, \rho, \omega} g_{3J/\psi} g^{\mu\alpha} \frac{(\not{q} + \not{p} + m_{N_{c\bar{c}}^*}) P_{\alpha\beta}^{\frac{3}{2}}(p+q)}{W^2 - m_{N_{c\bar{c}}^*}^2 + i\Gamma_{N_{c\bar{c}}^*} m_{N_{c\bar{c}}^*}} F_V(0) \\ &\times \frac{ie}{f_V - m_V^2 + i\Gamma_V m_V} \frac{-m_V^2 \tilde{g}_{3V}}{m_V} \left(g^{\beta\nu} - \frac{3}{2} \frac{\tilde{r}^\beta \tilde{r}^\nu}{\tilde{r}^2} + \frac{1}{2} \tilde{g}_{N^*}^{\beta\nu} \right), \end{aligned} \quad (31)$$

$$\begin{aligned} \mathcal{M}_{N^*(\frac{5}{2}^+)}^{\mu\nu}(q, p, q', p') &= \sum_{V=J/\psi, \rho, \omega} \frac{g_{5J/\psi}}{m_N} g^{\mu\alpha} \tilde{r}^\beta \frac{(\not{q} + \not{p} + m_{N_{c\bar{c}}^*}) P_{\alpha\beta\alpha'\beta'}^{\frac{5}{2}}(p+q)}{W^2 - m_{N_{c\bar{c}}^*}^2 + i\Gamma_{N_{c\bar{c}}^*} m_{N_{c\bar{c}}^*}} F_V(0) \\ &\times \frac{ie}{f_V - m_V^2 + i\Gamma_V m_V} \frac{-m_V^2 \tilde{g}_{5V}/m_N}{m_N} \\ &\times \left(g^{\nu\alpha'} \tilde{r}^{\beta'} - \frac{5}{3} \frac{\tilde{r}^\nu \tilde{r}^{\alpha'} \tilde{r}^{\beta'}}{\tilde{r}^2} + \frac{1}{3} \left(\tilde{g}_{N^*}^{\nu\alpha'} \tilde{r}^{\beta'} + \tilde{g}_{N^*}^{\nu\beta'} \tilde{r}^{\alpha'} + \tilde{g}_{N^*}^{\alpha'\beta'} \tilde{r}^\nu \right) \right), \end{aligned} \quad (32)$$

where $P_{\alpha\beta}^{\frac{3}{2}}(p)$ and $P_{\alpha\beta\alpha'\beta'}^{\frac{5}{2}}(p)$, are the Lorentz structure functions of propagators of 3/2 and 5/2 particles, respectively. Their formulas are [100]:

$$P_{\alpha\beta}^{\frac{3}{2}}(p) = -g_{\alpha\beta} + \frac{1}{3} \gamma_\mu \gamma_\nu + \frac{2}{3} \frac{p_\mu p_\nu}{m_{N^*}^2} + \frac{1}{3m_{N^*}} (\gamma_\mu p_\nu - \gamma_\nu p_\mu) \quad (33)$$

$$\begin{aligned} P_{\alpha\beta\alpha'\beta'}^{\frac{5}{2}}(p) &= \frac{1}{2} (\tilde{g}_{N^*}^{\alpha\alpha'} \tilde{g}_{N^*}^{\beta\beta'} + \tilde{g}_{N^*}^{\alpha\beta'} \tilde{g}_{N^*}^{\beta\alpha'}) - \frac{1}{5} \tilde{g}_{N^*}^{\alpha\beta} \tilde{g}_{N^*}^{\alpha'\beta'} \\ &- \frac{1}{10} \left(\tilde{\gamma}^\alpha \tilde{\gamma}^{\alpha'} \tilde{g}_{N^*}^{\beta\beta'} + \tilde{\gamma}^\alpha \tilde{\gamma}^{\beta'} \tilde{g}_{N^*}^{\beta\alpha'} + \tilde{\gamma}^\beta \tilde{\gamma}^{\alpha'} \tilde{g}_{N^*}^{\alpha\beta'} + \tilde{\gamma}^\beta \tilde{\gamma}^{\beta'} \tilde{g}_{N^*}^{\alpha\alpha'} \right) \end{aligned} \quad (34)$$

III. PREDICTIONS FOR $\gamma p \rightarrow J/\psi p$

In this section, we will first use the available total cross section data to fix the cutoff parameter Λ of the off-shell form factor Eq.(28) of the $\gamma p \rightarrow N_{c\bar{c}}^*$ amplitude. We then make predictions for using differential cross sections for identifying the $N_{c\bar{c}}^*$ from the future experimental data.

A. Total cross section

From Fig.3, we see that the available data of the $\gamma p \rightarrow J/\psi p$ in the near threshold region are below about 0.8 nb and have some structure which may be due to the experimental

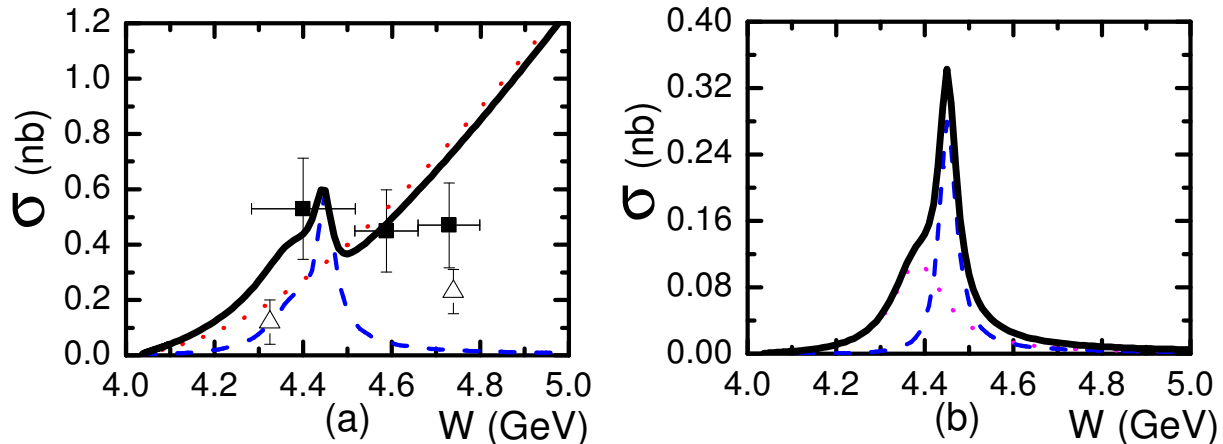


FIG. 5: The total cross sections of $\gamma p \rightarrow J/\psi p$ diagram with the invariant mass of γp . (a) The red dotted and blue dashed curves are the contribution from the Pomeron-exchange and $N_{c\bar{c}}^*$ with $J^p = 3/2^-$ and $5/2^+$ with $\Lambda = 550$ MeV, respectively. The black solid line is for the coherent summation of all above three contributions. (b) The red dotted and blue dashed curves are the contribution of $N_{c\bar{c}}^*$ with $J^p = 3/2^-$ and $5/2^+$ with $\Lambda = 550$ MeV, respectively. The solid black line is the coherent summation of two $N_{c\bar{c}}^*$ and it is the same as blue dashed curve in Fig.(a) here. The experimental data is from Refs. [95, 96].

uncertainties, but may be due to the $N_{c\bar{c}}^*$ excitations. In this section we will make predictions for investigating the extent to which these available data can accommodate the the $N_{c\bar{c}}^*$ excitations predicted by the models listed in Table I and II. In particular, we are interested in the predictions of Ref.[42] since this is the only model which predicts the partial decay width to γp channel for the $\frac{3}{2}^-$ (4380) and $\frac{5}{2}^+$ (4450) states. The tri-angular mechanism they used for the $\gamma N \rightarrow N_{c\bar{c}}^*$ (4380) is similar as our model based on VMD, but for $N_{c\bar{c}}^*$ (4450) they are different with one magnitude order.

Our first step is to determine the cutoff parameter Λ of the off-shell form factor Eq.(28). To compare with the results of Ref.[42], we perform calculations including only $\frac{3}{2}^-$ (4380) and $\frac{5}{2}^+$ (4450) using the parameters (No. 9 and 18 of Ref.[42]) listed in Table III. We find that the calculated total cross sections can be close to the available data shown in Fig.3 if we choose the cutoff in the range of $500 \text{ MeV} \leq \Lambda \leq 650 \text{ MeV}$. In Fig.5(a), we see that the choice $\Lambda = 550$ MeV gives results within the uncertainties of the available data. The structure of the solid curve at $W \sim 4.35$ GeV is due to the interference between the Pomeron-exchange amplitude (dotted curve) and the resonant amplitude (long dashed curve). Furthermore, we also see that the resonant amplitude is dominated by the $\frac{5}{2}^+$ (4450), as shown in Fig.5(b).

With the same cutoff $\Lambda = 550$ MeV, we then calculate $\Gamma_{N_{c\bar{c}}^* \rightarrow \gamma N}$ for all states, as listed in Table III. With the widths given in Table III, we then estimate the total cross sections of $\gamma p \rightarrow N_{c\bar{c}}^* \rightarrow J/\psi p$ by using Eq.(11) for all models. We can see in the last column of Table III that except the $\frac{3}{2}^-$ (4380) and $\frac{5}{2}^+$ (4450) of Ref.[42], all of the estimated total cross sections are either too large or too small compared with the value ~ 0.5 nb of the available data shown in Fig.5.

In Table IV, we compare our results of $\Gamma_{\gamma p}$ and $\sigma^{(tot)}$ of $\gamma p \rightarrow N_{c\bar{c}}^* \rightarrow J/\psi p$ with those

TABLE IV: fitting the partial decay widths of the states included in our predictions. $\Gamma_{\gamma p}$ are partial decay widths calculated from \tilde{g}_V within VMD, as explained in the text. $\sigma^{(tot)}$ is the total cross section of $\gamma p \rightarrow J/\psi p$ calculated from using Eq.(20) by choosing $\Lambda = 0.55$ GeV for the off-shell form factor $F_V(q^2)$.

No.	J^P	m	Γ_{tot}	$\Gamma_{J/\psi p}$	$\Gamma_{p\gamma}$ (keV)	$\sigma^{(tot)}$ (nb)	Ref.
9	$\frac{3}{2}^-$	4380	144.3	3.8	0.53	0.11	This work
		4380	144, 3	3.8	0.70	0.15	[42]
18	$\frac{5}{2}^+$	4450	46.4	4.0	0.083	0.25	This work
		4450	46.4	4.0	1.13	3.4	[42]

of Ref.[42]. Here we see that our result for the $\frac{5}{2}^+$ (4450) is much smaller than theirs. The differences between this work and Ref. [42] are from using rather different mechanisms to evaluate $\gamma N \rightarrow N_{c\bar{c}}^*$. It is therefore useful to examine how our predictions depend on the parameters of our model based on VMD. We first examine the the contribution from each of the intermediate vector mesons, illustrated in Fig.4, to the calculated total cross sections of $\gamma p \rightarrow N_{c\bar{c}}^* \rightarrow J/\psi p$. Our results from including the $J = \frac{3}{2}^-$ (4380) and $\frac{5}{2}^+$ (4450) in the calculation are shown in Fig.6. Clearly the intermediate ρ gives the largest contribution, and J/ψ is negligible. This can be understood from the employed off-shell form factor Eq.(28) which depends on the mass of the intermediate vector meson. This is also the reason why the cross sections predicted by the models without ρp channel listed in Table.III are extremely small.

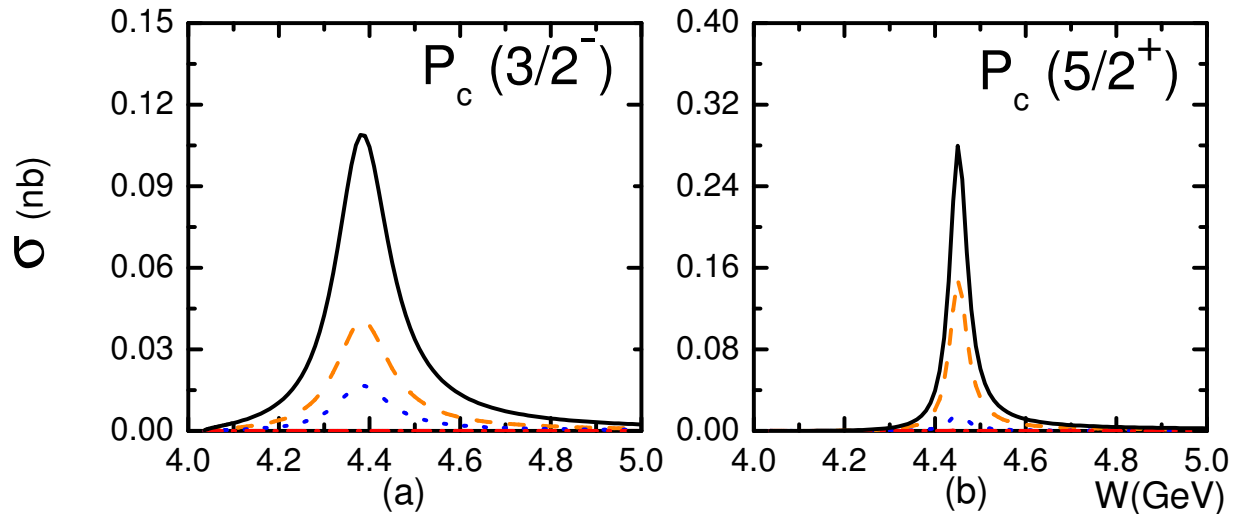


FIG. 6: The cross sections of $\gamma p \rightarrow N_{c\bar{c}}^* \rightarrow J/\psi p$ diagram for different J^P of $N_{c\bar{c}}^*$ with the invariant mass of γp . The orange dashed, blue dotted and red dashed-dotted lines are the contribution purely from the VMD by ρ , ω and J/ψ coupled with γ , respectively. The black solid lines are for the coherent summation of ρ , ω and J/ψ contributions.

B. differential cross sections

In Fig.5, we see that the feature of $N_{c\bar{c}}^*$ excitation in the total cross section is not so pronounced because it interfere with the background from Pomeron-exchange amplitude which is very large in all energy region. To extract the peak of $N_{c\bar{c}}^*$, we need to find other observables which are not dominated by the Pomeron exchange. It is noticed that the Pomeron exchange is strongly suppressed with large t in Eq.(10). In other word, the Pomeron-exchange mainly contribute to the cross sections at forward angles. This is illustrated in Fig.7. It is then clear that the resonance peaks will be easier to observe at large angles. This is illustrated in Fig.8. At 60° , the shoulder due to $N_{c\bar{c}}^*(4380)$ shows up more clearly. However, the magnitudes of the differential cross sections decrease rather rapidly with angles. Thus the measurement around 30° may be optimal in examining the existence $N_{c\bar{c}}^*$.

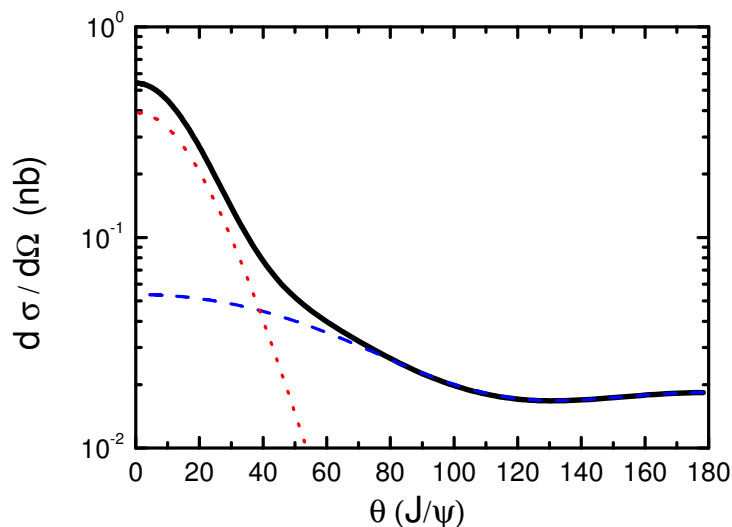


FIG. 7: The differential cross sections of $\gamma p \rightarrow J/\psi p$ diagram with the angular of outgoing J/ψ at invariant mass of γp $W = 4.45$ GeV. The red dotted, blue dashed lines are the contribution purely from the Pomeron and $N_{c\bar{c}}^*$ with $\Lambda = 0.55$ GeV, respectively. The black solid line is for the coherent summation of all contributions.

IV. PREDICTION ON $\gamma p \rightarrow \bar{D}^0 \Lambda_c^+, \bar{D}^{*0} \Lambda_c^+$

It is important to note that Pomeron-exchange amplitude is still dominant in determining the J/ψ production in the considered low energy region. Therefore it is interesting to test the VMD model of $\gamma N \rightarrow N_{c\bar{c}}^*$ by other reactions which do not have Pomeron-exchange mechanism and in the low energy region accessible to experiments measuring J/ψ production at JLab. With the $N_{c\bar{c}}^*$ models No. 6, 9, and 18 selected from Table II and listed in Table V, the reaction $\gamma p \rightarrow \bar{D}^{*0} \Lambda_c^+, \bar{D}^0 \Lambda_c^+$ can be used for this purpose. In addition to calculating the $\gamma p \rightarrow N_{c\bar{c}}^* \rightarrow \bar{D}^{*0} \Lambda_c^+, \bar{D}^0 \Lambda_c^+$ amplitude, we also need to consider the meson-exchange mechanisms due to $\bar{D}^{*0} \rightarrow \bar{D}^0 \gamma$ process. We thus need to calculate the amplitudes of the two mechanisms shown in Fig. 10.

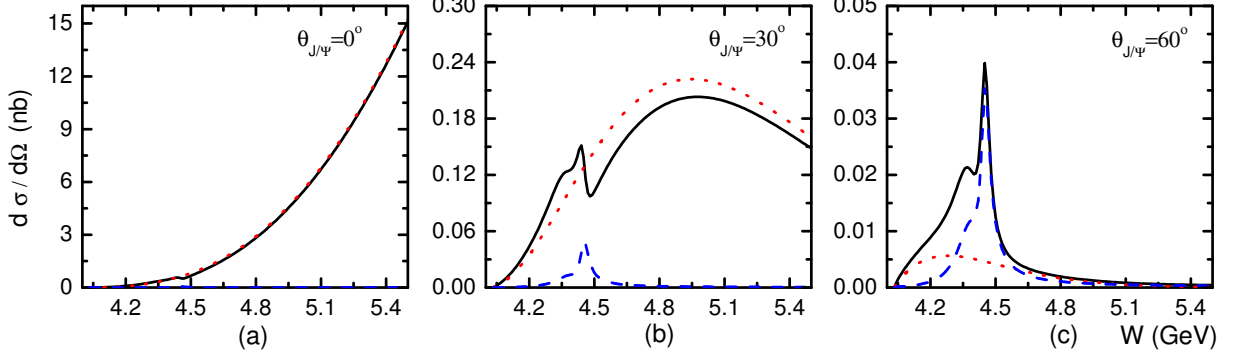


FIG. 8: The differential cross sections of $\gamma p \rightarrow J/\psi p$ diagram with invariant mass of γp at three fixed angular of outgoing J/ψ . The red dotted, blue dashed lines are the contribution purely from the Pomeron-exchange and $N_{c\bar{c}}^*$ with $\Lambda = 0.55$ GeV, respectively. The black solid line is for the coherent summation of all contributions.

A. meson-exchange amplitude

The meson-exchange amplitudes shown in Fig. 10 (b) can be calculated by using $D^*D\gamma$, $pD^*\Lambda_c^+$ and $pD^0\Lambda_c^+$ vertices defined as follows:

$$\mathcal{M}_{D^*D\gamma} = \frac{g_{D^*D^0\gamma}}{\sqrt{m_{D^*}m_D}} \epsilon^{\mu\nu\alpha\beta} P_{\gamma\mu} \epsilon_{\gamma\nu} P_{D^*\alpha} \epsilon_{D^*\nu}, \quad (35)$$

$$\mathcal{M}_{ND\Lambda_c^+} = g_{ND\Lambda_c^+} \bar{u}_{\Lambda_c^+} \gamma_5 u_N, \quad (36)$$

$$\mathcal{M}_{ND^*\Lambda_c^+} = g_{ND^*\Lambda_c^+} \bar{u}_{\Lambda_c^+} \gamma_\mu \epsilon_{D^*\mu} u_N, \quad (37)$$

where coupling $g_{D^*D^0\gamma} = 1.07$ is calculated from partial decay width of $D^{*0} \rightarrow D^0\gamma$ which is estimated from the measured ratio of widths $\Gamma_{D^{*0} \rightarrow D^0\gamma} / \Gamma_{D^{*0} \rightarrow D^0\pi^0}$ with $\Gamma_{D^{*0} \rightarrow D^0\pi^0}$ obtained from the data of $\Gamma_{D^{*+} \rightarrow D^+\pi^0}$ by using isospin. By using SU(4) symmetry [101], the coupling constants in Eqs.(36)-(37) can be determined: $g_{ND\Lambda_c^+} = -\frac{3\sqrt{3}}{5}g_{BBP}$ and $g_{ND^*\Lambda_c^+} = -\sqrt{3}g_{BBV}$, where $g_{BBP} = 0.989$ and $g_{BBV} = 3.25$. Then the amplitude $j_{D^* m'_s, m_s}^\nu(q, p, q', p')$, defined in Eq.(3), for $\gamma p \rightarrow \bar{D}^0\Lambda_c^+$ due to \bar{D}^{*0} -exchange can be written as

$$j_{D^* m'_s, m_s}^\nu(q, p, q', p') = \frac{g_{D^*D\gamma} g_{ND^*\Lambda_c^+}}{\sqrt{m_{D^*}m_D}} \epsilon^{\mu\nu\alpha\beta} \frac{q_\mu q'_\alpha \bar{u}_{\Lambda_c^+}(p', m'_s) \gamma_\beta u_p(p, m_s)}{(q' - q)^2 - m_{D^*}^2} F_{D^*}(q' - q). \quad (38)$$

Similarly, the \bar{D}^0 -exchange amplitude for $\gamma p \rightarrow \bar{D}^{*0}\Lambda_c^+$ is

$$j_{\bar{D}^0 m'_s, m_s}^\nu(q, p, q', p') = \frac{g_{D^*D\gamma} g_{ND\Lambda_c^+}}{\sqrt{m_{D^*}m_D}} \epsilon^{\mu\nu\alpha\beta} \frac{q_\mu q'_\alpha \epsilon_{D^*\beta} \bar{u}_{\Lambda_c^+}(p', m'_s) \gamma_5 u_p(p, m_s)}{(q' - q)^2 - m_{D^*}^2} F_{\bar{D}^0}(q' - q), \quad (39)$$

B. $N_{c\bar{c}}^*$ -excitation amplitudes

The formula for calculating the resonant amplitude $\gamma N \rightarrow N_{c\bar{c}}^* \rightarrow \Lambda_c^+ \bar{D}^*$ are the same as Eqs.(30)-(32) except that the coupling constants $g_{2JJ/\psi}$ for $J = 1/2, 3/2, 5/2$ are replaced by $g_{N^* \rightarrow \bar{D}\Lambda}$ for each J listed in Table V.

For the $\gamma N \rightarrow N_{c\bar{c}}^* \rightarrow \Lambda_c^+ \bar{D}$, we define $N_{c\bar{c}}^* \Lambda_c^+ \bar{D}$ vertices as follows:

$$\mathcal{M}_{N_{c\bar{c}}^*(\frac{1}{2}^-) \Lambda_c^+ \bar{D}} = g_1 \bar{u}_{\Lambda_c^+} u_{N_{c\bar{c}}^*}, \quad (40)$$

$$\mathcal{M}_{N_{c\bar{c}}^*(\frac{3}{2}^-) \Lambda_c^+ \bar{D}} = \frac{g_3}{m_D^2} \bar{u}_{\Lambda_c^+} \gamma_5 \gamma_\mu u_{N_{c\bar{c}}^*} \nu p_D^\mu p_D^\nu, \quad (41)$$

$$\mathcal{M}_{N_{c\bar{c}}^*(\frac{5}{2}^+) \Lambda_c^+ \bar{D}} = \frac{g_5}{m_D^3} \bar{u}_{\Lambda_c^+} \gamma_5 \gamma_\mu u_{N_{c\bar{c}}^*} \nu \lambda p_D^\mu p_D^\nu p_D^\lambda, \quad (42)$$

where $p_{\bar{D}}$ is the four momentum of \bar{D} meson. The coupling can be calculated from the partial decay widths listed in No. 6, 9, and 18 of Tab.V. We then get $g_1 = 0.40$, $g_3 = 1.29$, and $g_5 = 13.39$.

With the above equations and the $\gamma p \rightarrow N_{c\bar{c}}^*$ given in Table III, we can calculate the amplitude for $\gamma p \rightarrow N_{c\bar{c}}^* \rightarrow \bar{D}^0 \Lambda_c^+$ and obtain the corresponding current matrix element $j_{N_{c\bar{c}}^* m'_s, m_s}^\nu(q, p, q', p')$ (defined in Eq.(3)) as:

$$\begin{aligned} j_{N_{c\bar{c}}^*(\frac{1}{2}^-) m'_s, m_s}^\nu(q, p, q', p') &= \sum_{V=J/\psi, \rho, \omega} g_1 \frac{\bar{u}_{\Lambda_c^+}(p', m'_s) (\not{q} + \not{p} + m_{N_{c\bar{c}}^*}) u_p(p, m_s)}{W^2 - m_{N_{c\bar{c}}^*}^2 + i\Gamma_{N_{c\bar{c}}^*} m_{N_{c\bar{c}}^*}} F_V(0) \\ &\times \frac{ie}{f_V} \frac{-m_V^2 \tilde{g}_{1V}}{-m_V^2 + i\Gamma_V m_V} \gamma_5 \tilde{\gamma}_\beta \left(g^{\beta\nu} - \frac{3}{2} \frac{\tilde{r}^\beta \tilde{r}^\nu}{\tilde{r}^2} + \frac{1}{2} \tilde{g}_{N_{c\bar{c}}^*}^{\beta\nu} \right), \end{aligned} \quad (43)$$

$$\begin{aligned} j_{N_{c\bar{c}}^*(\frac{3}{2}^-) m'_s, m_s}^\nu(q, p, q', p') &= \sum_{V=J/\psi, \rho, \omega} \frac{g_3}{m_D^2} \frac{\bar{u}_{\Lambda_c^+}(p', m'_s) \gamma_5 \not{q}' (\not{q} + \not{p} + m_{N_{c\bar{c}}^*}) P_{\alpha\beta}^{\frac{3}{2}}(p+q) u_p(p, m_s)}{W^2 - m_{N_{c\bar{c}}^*}^2 + i\Gamma_{N_{c\bar{c}}^*} m_{N_{c\bar{c}}^*}} \\ &\times q'^\alpha F_V(0) \frac{ie}{f_V} \frac{-m_V^2 \tilde{g}_{3V}}{-m_V^2 + i\Gamma_V m_V} \left(g^{\beta\nu} - \frac{3}{2} \frac{\tilde{r}^\beta \tilde{r}^\nu}{\tilde{r}^2} + \frac{1}{2} \tilde{g}_{N_{c\bar{c}}^*}^{\beta\nu} \right), \end{aligned} \quad (44)$$

$$\begin{aligned} j_{N_{c\bar{c}}^*(\frac{5}{2}^+) m'_s, m_s}^\nu(q, p, q', p') &= \sum_{V=J/\psi, \rho, \omega} \frac{g_5}{m_D^3} \frac{\bar{u}_{\Lambda_c^+}(p', m'_s) \gamma_5 \not{q}' (\not{q} + \not{p} + m_{N_{c\bar{c}}^*}) P_{\alpha\beta\alpha'\beta'}^{\frac{5}{2}}(p+q) u_p(p, m_s)}{W^2 - m_{N_{c\bar{c}}^*}^2 + i\Gamma_{N_{c\bar{c}}^*} m_{N_{c\bar{c}}^*}} \\ &\times q'^\alpha q'^\beta F_V(0) \frac{ie}{f_V} \frac{-m_V^2 \tilde{g}_{5V}/m_N}{-m_V^2 + i\Gamma_V m_V} \\ &\times \left(g^{\nu\alpha'} \tilde{r}^{\beta'} - \frac{5}{3} \frac{\tilde{r}^\nu \tilde{r}^{\alpha'} \tilde{r}^{\beta'}}{\tilde{r}^2} + \frac{1}{3} \left(\tilde{g}_{N_{c\bar{c}}^*}^{\nu\alpha'} \tilde{r}^{\beta'} + \tilde{g}_{N_{c\bar{c}}^*}^{\nu\beta'} \tilde{r}^{\alpha'} + \tilde{g}_{N_{c\bar{c}}^*}^{\alpha'\beta'} \tilde{r}^\nu \right) \right), \end{aligned} \quad (45)$$

C. Predictions of total cross sections

The predicted total cross section of $\gamma p \rightarrow N_{c\bar{c}}^* \rightarrow \bar{D}^0(\bar{D}^{*0}) \Lambda_c^+$ are shown in Fig.10. All calculations are done with cutoff $\Lambda = 550$ MeV, as determined in the previous sections for J/ψ production. We first find that the meson-exchange contributions (dotted-dotted-dashed) to the predicted total cross section of $\gamma p \rightarrow N_{c\bar{c}}^* \rightarrow \bar{D}^0(\bar{D}^{*0}) \Lambda_c^+$ are very weak. The contribution from $N_{c\bar{c}}^*(\frac{3}{2}^-)$ (blue dashed) is larger than that of $N_{c\bar{c}}^*(\frac{5}{2}^-)$ (orange dotted). Clearly, if the predicted cross section given in Fig.10 can be measured, it will provide an additional test of the prediction of $N_{c\bar{c}}^*(\frac{3}{2}^-)$ state. Hopefully such measurements can be made in the near future as an additional test of our prediction on J/ψ production, presented in the previous section.

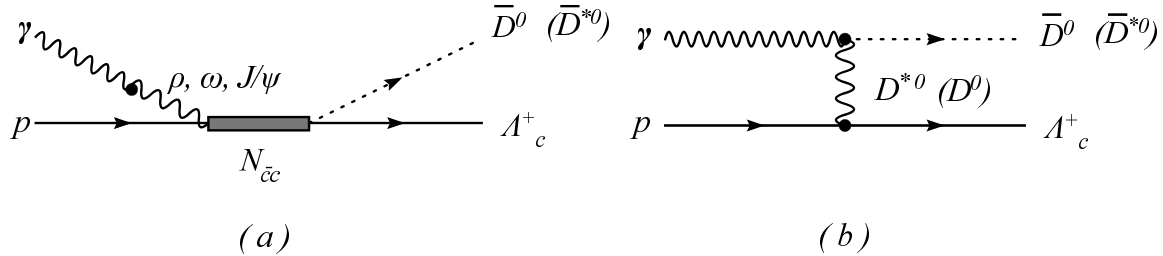


FIG. 9: The diagram (a) for $\gamma p \rightarrow N_{c\bar{c}} \rightarrow \bar{D}^0(\bar{D}^{*0})\Lambda_c^+$ with the VMD by ρ , ω and J/ψ coupled with γ , and (b) for $\gamma p \rightarrow \bar{D}^0(\bar{D}^{*0})\Lambda_c^+$ by exchanging $D^{*0}(D^0)$.

V. SUMMARY

By using the predictions from the available meson-baryon coupled-channel models, we have investigated the excitations of nucleon resonances with hidden charm, $N_{c\bar{c}}^*$, in the γp reactions. For the $\gamma p \rightarrow J/\psi p$ process, the Pomeron-exchange model of Donnachie and Landshoff, with the parameters determined from fitting the available total cross section data up to $W = 300$ GeV, is used to calculate the non-resonant amplitudes. The resonant $\gamma p \rightarrow N_{c\bar{c}}^* \rightarrow J/\psi p$ amplitudes are calculated by using (1) the partial decay widths predicted by the considered meson-baryons coupled-channel models to evaluate the $N_{c\bar{c}}^* \rightarrow MB$ transition matrix elements, and (2) the Vector Meson Dominance (VMD) model to evaluate $\gamma p \rightarrow N_{c\bar{c}}^*$ as $\gamma p \rightarrow V p \rightarrow N_{c\bar{c}}^*$ with $V = \rho, \omega, J/\psi$. The predictions from adding these two amplitudes then depend on an off-shell form factor $F_V(q^2) = \lambda^4/(\Lambda^4 + (q^2 - m_V^2)^2)$ which is needed to account for the q^2 -dependence of VMD model. We find that with $\Lambda = 0.55$ GeV, the predicted total cross sections of $\gamma p \rightarrow J/\psi p$ are within the range of the available data in the energy region near J/ψ production threshold. We then demonstrate that the $N_{c\bar{c}}^*$ can be most easily identified in the differential cross sections at large angles where the contribution from Pomeron-exchange becomes negligible.

With the same VMD model and the same coupled-channel model of $N_{c\bar{c}}^*$, we then predict the cross sections of $\gamma p \rightarrow \bar{D}^0\Lambda_c^+(\bar{D}^{*0}\Lambda_c^+)$. We suggest that experiments on these reactions can be more effective to study $N_{c\bar{c}}^*$ since their non-resonant amplitudes, due to the exchange of $\bar{D}^{*0}(\bar{D}^0)$, are found to be very weak.

The most unsatisfactory aspect of this work is the phenomenological determination of the off-shell form factor $F_V(q^2)$. It is determined by only using the data of total cross sections of $\gamma p \rightarrow J/\psi p$ near the threshold, shown in Fig.3. While our predictions could be used as a first-step to determine whether the $N_{c\bar{c}}^*$ predicted by the available meson-baryon

TABLE V: The coupling of $g_{N^* \rightarrow \bar{D}\Lambda_c}$ and $g_{\bar{D}^*\Lambda_c}$ are used in the calculation.

No.	J^P	m	$\Gamma_{\bar{D}\Lambda_c}$	$g_{N^* \rightarrow \bar{D}\Lambda_c}$	$\Gamma_{\bar{D}^*\Lambda_c}$	$g_{N^* \rightarrow \bar{D}^*\Lambda_c}$	Ref.
6	$\frac{1}{2}^-$	4481	1.02	0.40	0.3	0.043	[17]
9	$\frac{3}{2}^-$	4380	1.2	1.29	131.3	1.90	[42]
18	$\frac{5}{2}^+$	4450	18.8	13.39	20.5	2.18	[42]

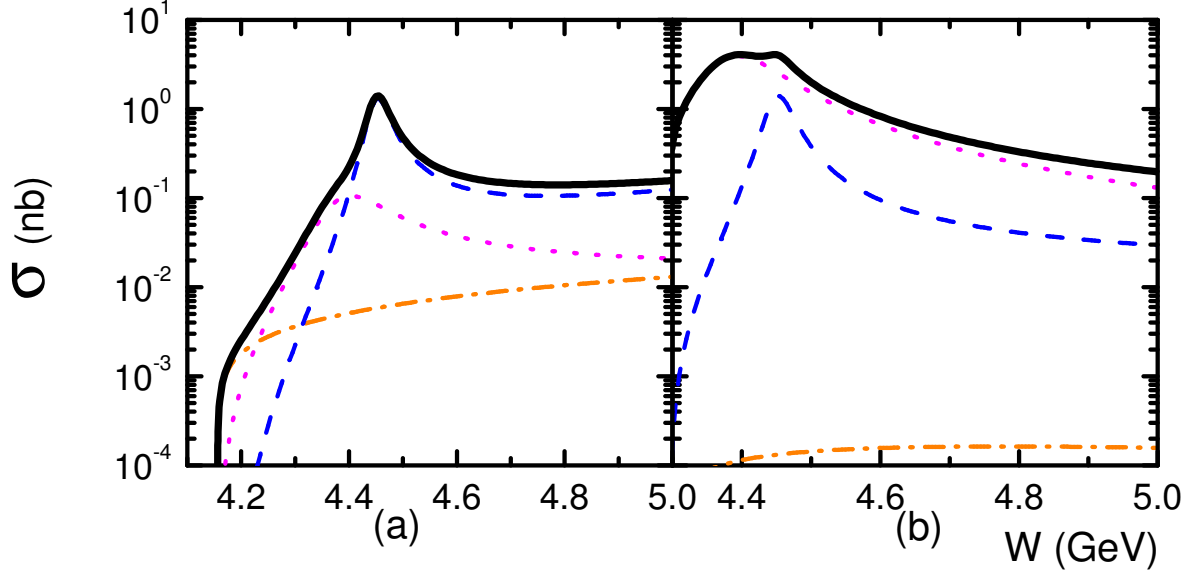


FIG. 10: The total cross sections of $\gamma p \rightarrow \bar{D}^0 \Lambda_c^+$ (a) and $\gamma p \rightarrow \bar{D}^{*0} \Lambda_c^+$ (b) with the invariant mass of γp . The pink dotted, blue dashed, orange dotted-dashed lines are the contribution purely from the $N_{c\bar{c}(\frac{3}{2}^-)}^*$, $N_{c\bar{c}(\frac{5}{2}^+)}^*$, and the background with $\Lambda = 0.55$ GeV, respectively. The black solid thick lines are for the coherent summation of all contributions with background $\Lambda = 0.55$ GeV.

coupled-channel models can be found in the new data from JLab, it is necessary to develop a more fundamental approach to also predict $F_V(q^2)$ from QCD models. Obviously, such an improvement is necessary for using the q^2 -dependence of the J/ψ electro-production cross section data to investigate nucleon resonances with hidden charm.

Acknowledgments

One of the authors Jia-jun Wu want to thanks the useful discussion with Hai-qing Zhou, Jun He, Jujun Xie, Qiang Zhao. This project is supported by the Thousand Talents Plan for Young Professionals and the National Natural Science Foundation of China under Grants No. 11621131001 (CRC110 cofunded by DFG and NSFC) and Grant No. 11835015. This work is also partially supported by the U.S. Department of Energy, Office of Science, Office of Nuclear Physics, Contract No. DE-AC02-06CH11357.

-
- [1] M. E. Peskin, Nucl. Phys. **B156**, 365 (1979).
 - [2] G. Bhanot and M. E. Peskin, Nucl. Phys. **B156**, 391 (1979).
 - [3] M. E. Luke, A. V. Manohar, and M. J. Savage, Phys. Lett. **B288**, 355 (1992), hep-ph/9204219.
 - [4] S. J. Brodsky and G. A. Miller, Phys. Lett. **B412**, 125 (1997), hep-ph/9707382.
 - [5] T. Kawanai and S. Sasaki, Phys. Rev. **D82**, 091501 (2010), 1009.3332.
 - [6] A. B. Kaidalov and P. E. Volkovitsky, Phys. Rev. Lett. **69**, 3155 (1992).
 - [7] A. Donnachie and P. V. Landshoff, Nucl. Phys. **B244**, 322 (1984), [,813(1984)].
 - [8] S. J. Brodsky, I. A. Schmidt, and G. F. de Teramond, Phys. Rev. Lett. **64**, 1011 (1990).
 - [9] J.-J. Wu and T. S. H. Lee, Phys. Rev. **C86**, 065203 (2012), 1210.6009.
 - [10] J.-J. Wu and T. S. H. Lee, Phys. Rev. **C88**, 015205 (2013), 1303.4967.
 - [11] J.-J. Wu, R. Molina, E. Oset, and B. S. Zou, Phys. Rev. Lett. **105**, 232001 (2010), 1007.0573.
 - [12] J.-J. Wu, R. Molina, E. Oset, and B. S. Zou, Phys. Rev. **C84**, 015202 (2011), 1011.2399.
 - [13] Z.-C. Yang, Z.-F. Sun, J. He, X. Liu, and S.-L. Zhu, Chin. Phys. **C36**, 6 (2012), 1105.2901.
 - [14] J.-J. Wu, T. S. H. Lee, and B. S. Zou, Phys. Rev. **C85**, 044002 (2012), 1202.1036.
 - [15] E. Oset, A. Ramos, E. J. Garzon, R. Molina, L. Tolos, C. W. Xiao, J. J. Wu, and B. S. Zou, Int. J. Mod. Phys. **E21**, 1230011 (2012), 1210.3738.
 - [16] C. Garcia-Recio, J. Nieves, O. Romanets, L. L. Salcedo, and L. Tolos, Phys. Rev. **D87**, 074034 (2013), 1302.6938.
 - [17] C. W. Xiao, J. Nieves, and E. Oset, Phys. Rev. **D88**, 056012 (2013), 1304.5368.
 - [18] T. Uchino, W.-H. Liang, and E. Oset, Eur. Phys. J. **A52**, 43 (2016), 1504.05726.
 - [19] S. G. Yuan, K. W. Wei, J. He, H. S. Xu, and B. S. Zou, Eur. Phys. J. **A48**, 61 (2012), 1201.0807.
 - [20] W. L. Wang, F. Huang, Z. Y. Zhang, and B. S. Zou, Phys. Rev. **C84**, 015203 (2011), 1101.0453.
 - [21] R. Aaij et al. (LHCb), Phys. Rev. Lett. **115**, 072001 (2015), 1507.03414.
 - [22] R. Aaij et al. (LHCb), Phys. Rev. Lett. **117**, 082003 (2016), [Addendum: Phys. Rev. Lett.118,119901(2017)], 1606.06999.
 - [23] R. Aaij et al. (LHCb) (2019), 1904.03947.
 - [24] R. Chen, X. Liu, X.-Q. Li, and S.-L. Zhu, Phys. Rev. Lett. **115**, 132002 (2015), 1507.03704.
 - [25] H.-X. Chen, W. Chen, X. Liu, T. G. Steele, and S.-L. Zhu, Phys. Rev. Lett. **115**, 172001 (2015), 1507.03717.
 - [26] L. Roca, J. Nieves, and E. Oset, Phys. Rev. **D92**, 094003 (2015), 1507.04249.
 - [27] J. He, Phys. Lett. **B753**, 547 (2016), 1507.05200.
 - [28] H. Huang, C. Deng, J. Ping, and F. Wang, Eur. Phys. J. **C76**, 624 (2016), 1510.04648.

- [29] G.-J. Wang, L. Ma, X. Liu, and S.-L. Zhu, Phys. Rev. **D93**, 034031 (2016), 1511.04845.
- [30] G. Yang and J. Ping, Phys. Rev. **D95**, 014010 (2017), 1511.09053.
- [31] R. Chen, X. Liu, and S.-L. Zhu, Nucl. Phys. **A954**, 406 (2016), 1601.03233.
- [32] L. Roca and E. Oset, Eur. Phys. J. **C76**, 591 (2016), 1602.06791.
- [33] Q.-F. Lvy and Y.-B. Dong, Phys. Rev. **D93**, 074020 (2016), 1603.00559.
- [34] Y. Shimizu, D. Suenaga, and M. Harada, Phys. Rev. **D93**, 114003 (2016), 1603.02376.
- [35] C.-W. Shen, F.-K. Guo, J.-J. Xie, and B.-S. Zou, Nucl. Phys. **A954**, 393 (2016), 1603.04672.
- [36] P. G. Ortega, D. R. Entem, and F. Fernandez, Phys. Lett. **B764**, 207 (2017), 1606.06148.
- [37] U.-G. Meissner and J. A. Oller, Phys. Lett. **B751**, 59 (2015), 1507.07478.
- [38] Y. Yamaguchi and E. Santopinto, Phys. Rev. **D96**, 014018 (2017), 1606.08330.
- [39] J. He, Phys. Rev. **D95**, 074004 (2017), 1607.03223.
- [40] E. Oset et al., Nucl. Phys. **A954**, 371 (2016).
- [41] C. W. Xiao, Phys. Rev. **D95**, 014006 (2017), 1609.02712.
- [42] Y.-H. Lin, C.-W. Shen, F.-K. Guo, and B.-S. Zou, Phys. Rev. **D95**, 114017 (2017), 1703.01045.
- [43] Y. Yamaguchi, A. Giachino, A. Hosaka, E. Santopinto, S. Takeuchi, and M. Takizawa, Phys. Rev. **D96**, 114031 (2017), 1709.00819.
- [44] C.-W. Shen, D. Ronchen, U.-G. Meissner, and B.-S. Zou, Chin. Phys. **C42**, 023106 (2018), 1710.03885.
- [45] Y.-H. Lin, C.-W. Shen, and B.-S. Zou, Nucl. Phys. **A980**, 21 (2018), 1805.06843.
- [46] Y. Shimizu, Y. Yamaguchi, and M. Harada (2019), 1901.09215.
- [47] J. Ferretti, E. Santopinto, M. Naeem Anwar, and M. A. Bedolla, Phys. Lett. **B789**, 562 (2019), 1807.01207.
- [48] M. I. Eides and V. Y. Petrov (2018), 1811.01691.
- [49] T. J. Burns, Eur. Phys. J. **A51**, 152 (2015), 1509.02460.
- [50] S. Takeuchi and M. Takizawa, Phys. Lett. **B764**, 254 (2017), 1608.05475.
- [51] J.-B. Xiang, H.-X. Chen, W. Chen, X.-B. Li, X.-Q. Yao, and S.-L. Zhu, Chin. Phys. **C43**, 034104 (2019), 1711.01545.
- [52] H. Li, Z.-X. Wu, C.-S. An, and H. Chen, Chin. Phys. **C41**, 124104 (2017).
- [53] E. Hiyama, A. Hosaka, M. Oka, and J.-M. Richard, Phys. Rev. **C98**, 045208 (2018), 1803.11369.
- [54] H.-X. Chen, E.-L. Cui, W. Chen, X. Liu, T. G. Steele, and S.-L. Zhu, Eur. Phys. J. **C76**, 572 (2016), 1602.02433.
- [55] R. F. Lebed, Phys. Lett. **B749**, 454 (2015), 1507.05867.
- [56] G.-N. Li, X.-G. He, and M. He, JHEP **12**, 128 (2015), 1507.08252.
- [57] Z.-G. Wang, Eur. Phys. J. **C76**, 70 (2016), 1508.01468.
- [58] R. Zhu and C.-F. Qiao, Phys. Lett. **B756**, 259 (2016), 1510.08693.
- [59] F.-K. Guo, U.-G. Meissner, W. Wang, and Z. Yang, Phys. Rev. **D92**, 071502 (2015), 1507.04950.
- [60] X.-H. Liu, Q. Wang, and Q. Zhao, Phys. Lett. **B757**, 231 (2016), 1507.05359.
- [61] F.-K. Guo, U. G. Meissner, J. Nieves, and Z. Yang, Eur. Phys. J. **A52**, 318 (2016), 1605.05113.
- [62] M. Bayar, F. Aceti, F.-K. Guo, and E. Oset, Phys. Rev. **D94**, 074039 (2016), 1609.04133.
- [63] H.-X. Chen, W. Chen, X. Liu, and S.-L. Zhu, Phys. Rept. **639**, 1 (2016), 1601.02092.
- [64] Q. Zhao, AAPPs Bull. **26**, 8 (2016).
- [65] Y. Dong, A. Faessler, and V. E. Lyubovitskij, Prog. Part. Nucl. Phys. **94**, 282 (2017).

- [66] F.-K. Guo, C. Hanhart, U.-G. Meissner, Q. Wang, Q. Zhao, and B.-S. Zou, *Rev. Mod. Phys.* **90**, 015004 (2018), 1705.00141.
- [67] A. Ali, J. S. Lange, and S. Stone, *Prog. Part. Nucl. Phys.* **97**, 123 (2017), 1706.00610.
- [68] R. Chen, Z.-F. Sun, X. Liu, and S.-L. Zhu (2019), 1903.11013.
- [69] H.-X. Chen, W. Chen, and S.-L. Zhu (2019), 1903.11001.
- [70] M.-Z. Liu, Y.-W. Pan, F.-Z. Peng, M. Sanchez Sanchez, L.-S. Geng, A. Hosaka, and M. Pavon Valderrama (2019), 1903.11560.
- [71] F.-K. Guo, H.-J. Jing, U.-G. Meissner, and S. Sakai (2019), 1903.11503.
- [72] J. He (2019), 1903.11872.
- [73] Y.-R. Liu, H.-X. Chen, W. Chen, X. Liu, and S.-L. Zhu (2019), 1903.11976.
- [74] H. Huang, J. He, and J. Ping (2019), 1904.00221.
- [75] C.-J. Xiao, Y. Huang, Y.-B. Dong, L.-S. Geng, and D.-Y. Chen (2019), 1904.00872.
- [76] Y. Shimizu, Y. Yamaguchi, and M. Harada (2019), 1904.00587.
- [77] Z.-H. Guo and J. A. Oller (2019), 1904.00851.
- [78] A. Ali and A. Ya. Parkhomenko (2019), 1904.00446.
- [79] Y. Huang, J. He, H.-F. Zhang, and X.-R. Chen, *J. Phys.* **G41**, 115004 (2014), 1305.4434.
- [80] Q. Wang, X.-H. Liu, and Q. Zhao, *Phys. Rev.* **D92**, 034022 (2015), 1508.00339.
- [81] V. Kubarovskiy and M. B. Voloshin, *Phys. Rev.* **D92**, 031502 (2015), 1508.00888.
- [82] M. Karliner and J. L. Rosner, *Phys. Lett.* **B752**, 329 (2016), 1508.01496.
- [83] A. N. Hiller Blin, C. Fernandez-Ramirez, A. Jackura, V. Mathieu, V. I. Mokeev, A. Pilloni, and A. P. Szczepaniak, *Phys. Rev.* **D94**, 034002 (2016), 1606.08912.
- [84] E. Ya. Paryev and Yu. T. Kiselev, *Nucl. Phys.* **A978**, 201 (2018), 1810.01715.
- [85] X.-Y. Wang, X.-R. Chen, and J. He (2019), 1904.11706.
- [86] Z. E. Meziani et al. (2016), 1609.00676.
- [87] K. Hafidi, S. Joosten, Z. E. Meziani, and J. W. Qiu, *Few Body Syst.* **58**, 141 (2017).
- [88] S. Dobbs (GlueX), *PoS Hadron2017*, 047 (2018), 1712.07214.
- [89] A. Ali et al. (GlueX) (2019), 1905.10811.
- [90] H. Kamano, S. X. Nakamura, T. S. H. Lee, and T. Sato, *Phys. Rev.* **D84**, 114019 (2011), 1106.4523.
- [91] M. A. Pichowsky and T. S. H. Lee, *Phys. Rev.* **D56**, 1644 (1997), nucl-th/9612049.
- [92] S. J. Brodsky, E. Chudakov, P. Hoyer, and J. M. Laget, *Phys. Lett.* **B498**, 23 (2001), hep-ph/0010343.
- [93] P. V. Landshoff and O. Nachtmann, *Z. Phys.* **C35**, 405 (1987).
- [94] Y.-s. Oh and T. S. H. Lee, *Phys. Rev.* **C66**, 045201 (2002), nucl-th/0204035.
- [95] B. Gittelman, K. M. Hanson, D. Larson, E. Loh, A. Silverman, and G. Theodosiou, *Phys. Rev. Lett.* **35**, 1616 (1975).
- [96] R. L. Anderson, in *International Conference on the Production of Particles with New Quantum Numbers Madison, Wis., April 22-24, 1976* (1976), p. 102, URL <http://www-public.slac.stanford.edu/sciDoc/docMeta.aspx?slacPubNumber=SLAC-PUB-1741>.
- [97] U. Camerini, J. G. Learned, R. Prepost, C. M. Spencer, D. E. Wisner, W. Ash, R. L. Anderson, D. Ritson, D. Sherden, and C. K. Sinclair, *Phys. Rev. Lett.* **35**, 483 (1975).
- [98] H. Huang and J. Ping, *Phys. Rev.* **D99**, 014010 (2019), 1811.04260.
- [99] B. S. Zou and F. Hussain, *Phys. Rev.* **C67**, 015204 (2003), hep-ph/0210164.
- [100] S. Dulat, J.-J. Wu, and B. S. Zou, *Phys. Rev.* **D83**, 094032 (2011), 1103.5810.
- [101] C.-W. Shen, J.-J. Wu, and B.-S. Zou (2019), 1906.03896.